

We are IntechOpen, the world's leading publisher of Open Access books Built by scientists, for scientists

6,900

Open access books available

186,000

International authors and editors

200M

Downloads

Our authors are among the

154

Countries delivered to

TOP 1%

most cited scientists

12.2%

Contributors from top 500 universities



WEB OF SCIENCE™

Selection of our books indexed in the Book Citation Index
in Web of Science™ Core Collection (BKCI)

Interested in publishing with us?
Contact book.department@intechopen.com

Numbers displayed above are based on latest data collected.
For more information visit www.intechopen.com



Magnetohydrodynamics in Biomedical Applications

*Hamid Farrokhi, David O. Otuya, Anna Khimchenko
and Jing Dong*

Abstract

This chapter discusses recent advances in biomedical applications of magnetohydrodynamics (MHD). The magnetohydrodynamic (MDH) effect is a physical phenomenon describing the motion of a conducting fluid flowing under influencing of an external magnetic field. The chapter covers four primary areas of research: (1) laser beam scanning, (2) nano-particle manipulation, (3) imaging contrast enhancement, and (4) targeted drug delivery. The state-of-the-art devices based on magnetohydrodynamic principles are also presented, providing a broad view of biomedical MHDs. As the field of biomedical MHDs continues to grow, advances towards micro-scale transitions will continue to be made, maintaining its clinically driven nature and motion towards real-world applications.

Keywords: magnetohydrodynamics, beam scanning, nanoparticles, imaging contrast, targeted drug delivery, magnetic constructs

1. Introduction

Magnetohydrodynamic (MDH) effect is a physical phenomenon that describes the motion of charge conducting fluid flowing which his influenced by an external magnetic field. Its applications have been studied extensively across multiple disciplines ranging from the study of solar winds [1, 2] to MHD-driven biomedical sensors [3] and actuators [4–7]. This chapter narrows the focus of MHD applications to biomedical sciences. The chapter introduces four primary MHD biomedical applications: (1) magnetohydrodynamic-based laser beam scanning, (2) nanoparticle manipulations for biomedical applications, (3) biomedical imaging contrast enhancement, and (4) targeted drug delivery.

This chapter aims to present the current state of the art in the field with regards to biomedical and clinical applications of the MHD effect.

2. Magnetohydrodynamic-based laser beam scanning

2.1 Introduction

Adaptive optics (AO) enables correcting of complex aberrations for a broad range of applications [1, 2]. Conventional AO systems use spatial light modulators [3, 4] or solid deformable mirrors (DM) [5, 6] to compensate the phase changes

resulting from non-uniformity in the properties of the medium through which light travels or from faults in the geometry of the component. There are two types of spatial light modulators operating in reflective and transmission modes. Due to using small liquid crystals, this type of wavefront shaping is able to provide very high spatial resolution. However, there is a limitation in the correction magnitude which is usually in the range of a few micrometers. To resolve this issue, solid deformable mirrors have been developed and adopted widely to correct wavefront in optical systems. It consists of a solid reflecting surface connected to an actuator structure. By controlling the actuators, the shape of the reflective surface can be changed to compensate the wavefront distortions. The high cost of the actuators and intricate fabrication process are the main problems of the solid deformable mirrors. The current solid deformable mirrors can only provide small inter-actuator strokes, with the maximum deflection in the range of tens of micrometers.

AO systems have been used in laser beam shaping [7–9] and eye imaging systems [10–12] to effectively address both the low-intensity high-order aberrations and the high-intensity low-order aberrations. For example, high-resolution retinal imaging using AO plays a vital role in vision science and will help the early clinical diagnosis of eye diseases. For dealing with the ocular aberrations for a large population, e.g., myopic eyes, adaptive optics using two deformable mirrors have been designed [10–12]. The large-stroke DM with a limited number of actuators is used to correct large-intensity low-order aberrations. The second DM with a low stroke and a high spatial correction resolution is used to address the small-intensity high-order aberrations. However, its application in ophthalmology is limited by the complexity and the high cost. A new type of liquid deformable mirror [13–15] has been designed based on the actuation of the magnetic fluid. Although the liquid mirrors are constrained to the horizontal setup, the magnetic fluid deformable mirrors (MFDM) offer large strokes, low cost, and easy fabrication. Using the single inter-actuator, the strokes more than 100 μm can be obtained with less power consumption. However, to produce a large mirror surface deformation, the size of the electromagnetic coils needs to be large. This makes the density of actuators low, and it is not suitable for high-order aberrations. A full-order correction with the high spatial resolution is achieved using a two-layer design layout with small electromagnetic coils. A new wavefront corrector, MFDM, has major advantages such as large stroke, low cost, easy fabrication process, which can be easily customized for different applications. In the following sections, we will explain the technology and possible applications in *in-vivo* imaging and probing.

2.2 Magnetic fluid deformable mirror (MFDM)

The main elements of the MFDM are a layer of magnetic fluid, a thin film of a reflective material coated on the free surface of the fluid, a two-layer layout of the miniature electromagnetic coils placed beneath the fluid layer, and a Maxwell coil(s) (see **Figure 1**). The properties of the magnetic fluid used in the study are given in **Table 1**. Based on the definition, the magnetic fluid is a stable colloidal suspension of nano-sized, single-domain ferri/ferromagnetic particles. The fluid can be coated with a silver liquid-like thin film to improve the reflectance.

To achieve the correction of full-order aberrations with a high spatial resolution, the new design of MFDM is presented (see **Figure 1** for the details). The upper layer actuators of small size and high density are used to compensate for small-amplitude high-order aberrations, and the lower layer actuators with big size and low density are used to correct for large amplitude low order aberrations. The electromagnetic coils are circular coils wound on a cylindrical core. **Table 2** shows the physical parameters of the coil. Each layer of the coil is arranged in a hexagonal array.

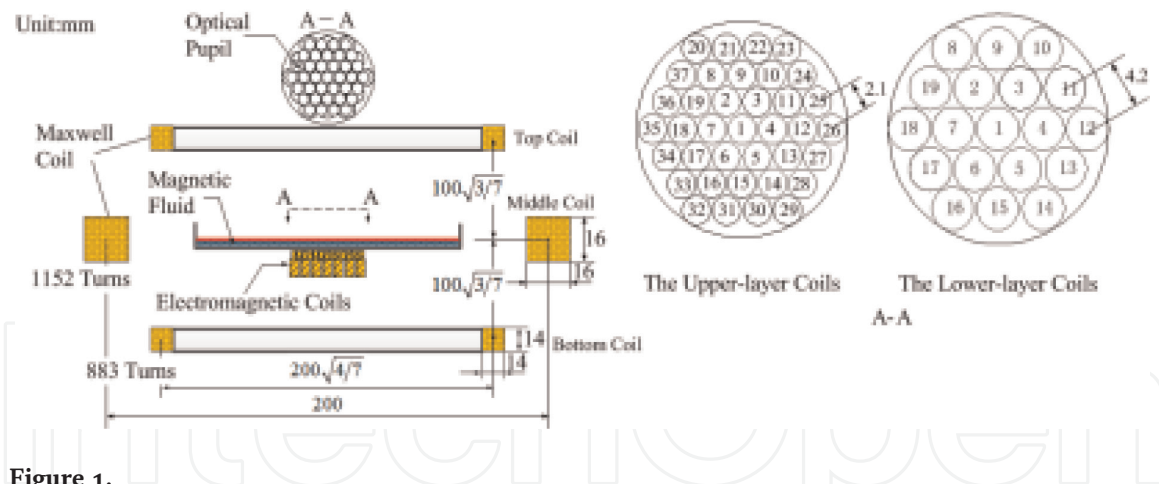


Figure 1. Schematic design of the magnetic fluid deformable mirror (MFDM) (adapted from [20]).

Magnetic fluid	Parameters
Saturation magnetization	22 mT
Relative permeability	2.89
Density	1190 kg/m ³
Viscosity	3 cp
Thickness	1 mm

Table 1. Parameters of the magnetic fluid.

Magnetic fluid	Parameters	
Position	Upper	Lower
Core-type	Air-cored	Air-cored
Material	Copper	Copper
Wire gauge	AWG37	AWG36
Internal diameter	1 mm	2 mm
External diameter	2 mm	4 mm
Length	1 mm	8 mm

AWG, American wire gauge.

Table 2. Parameters of the miniature electromagnetic coil.

The upper layer coils are radially spaced at 2.1 mm from the center to center, and the lower layer coils are radially spaced at 4.2 mm, respectively.

To make the response of the actuators linear, the Maxwell coil was used to apply an external uniform magnetic field. The Maxwell coil consists of three individual coils, where both lateral/outer coils should have a radius of $\sqrt{4/7} R$, at a distance of $\sqrt{3/7} R$ from the middle coil with a radius of $R = 100$ mm [16] (see **Figure 1**).

Table 3 shows the parameters of the coil. The three coils are wired using American wire gauge (AWG) 25 magnet wire. The turn ratio of 64:49 is used for the top and bottom coils relative to the middle coil [16]. Also, magnetic fluids typically show low reflectance to light and can be coated with silver liquid-like thin films to improve the reflectance [17, 18]. The self-assembly method has been usually used to

Magnetic fluid	Parameters
Nominal diameter of the middle coil	200 mm
No. of turns in the middle coil	1152
No. of turn in the top and bottom coil	883
Average resistance of the middle coil	71.2 Ω
Average resistance of the coils	42.3 Ω
Wire gauge	AWG 25
Wire material	Copper
Bobbin material	Aluminum

Table 3.
Parameters of the Maxwell coil(s).

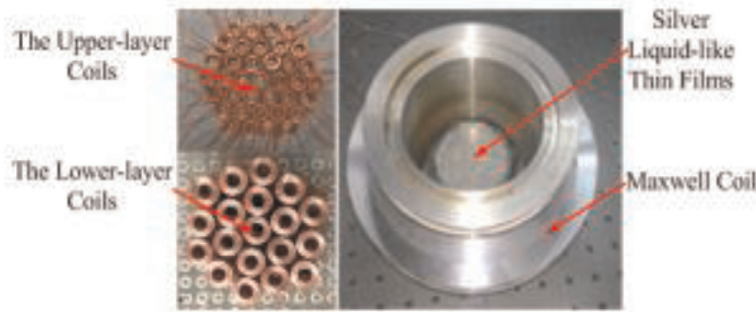


Figure 2.
Assembly of the prototype MFDM (adapted from [20]).

prepare the silver liquid-like thin film for the MFDM. Firstly, the solution of silver nanoparticles was dissociated by centrifugation to remove the supernatant, and ethanol was then infused to purify the silver nanoparticles. The obtained silver nanoparticles were mixed with the ethanol/dodecanethiol solution, kept at room temperature for 24 h, and then centrifuged. Then the ethyl acetate was added into the silver nanoparticles obtained from the previous step. This solution was then applied to the surface of the magnetic fluid. When the ethyl acetate evaporated, the hydrophobic dodecanethiol encapsulated silver nano-particles automatically stacked and spread on the surface of the magnetic fluid to form a large scale area of silver liquid-like film.

Figure 2 shows the fabricated mirror in which two-layer layout of the coils are installed within the Maxwell coil. Ferrofluid with layer thickness of about 1 mm is placed on top of the miniature coils, which is coated with the thin silver liquid-like film.

2.3 Working principle of MFDM

The MFDM is demonstrated by a cylindrical layer of a magnetic fluid as shown in **Figure 3**. The top free surface of the fluid layer is coated with a reflective film to be the deformable surface of the mirror. The surface deflection at the point (r_k, θ_k) is indicated by $\zeta(r_k, \theta_k, t)$, where $k = 1, 2, 3, \dots$, k is a discrete number of surface points. The magnetic field produced by any specific coil, centered at the horizontal location (r_{ij}, θ_{ij}) , is idealized as that of a point source of magnetic potential $\psi_{ij}(t)$, where $i = 1, 2$ is the i th layer of actuators, and $j, j = 1, 2, 3, \dots$, J_i is the j th coil of each layer.

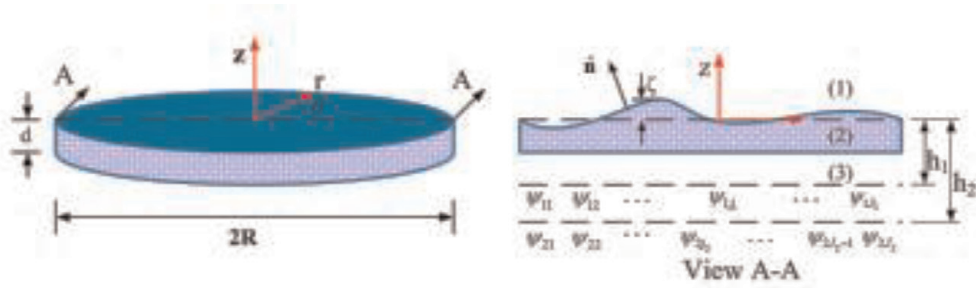


Figure 3.
 Geometric representation of a circular MFDM (adapted from [20]).

Maxwell's equations govern the magnetic field. Since the magnetic field of the miniature coils is taken as point sources of magnetic potential located at the fluid boundary, electromagnetic field can be considered as a current-free one. Using this assumption, the displacement currents in the fluid are negligible, Maxwell's equations can be written as:

$$\nabla \times H = 0, \nabla \cdot B = 0 \quad (1)$$

where B is the magnetic flux density, which is related to the magnetic field H and the magnetization M by the following equation:

$$B = \mu H = \mu_0 (H + M) \quad (2)$$

μ and μ_0 are the magnetic permeability of the magnetic fluid and free space, respectively. Assuming the applied field linearly magnetizes the magnetic fluid, the magnetization vector M can be written as

$$M = \chi H \quad (3)$$

where $\chi = \mu/\mu_0 - 1$ is considered to be constant. Considering that the magnetic field extends into space above and below the fluid layer, Maxwell's equations are applied to all three sub-domains (1)–(3) as shown in **Figure 3**. The scalar potentials $\psi^{(l)}$, $l = 1, 2, 3$ describe the magnetic field vectors $H^{(l)}$ in these sub-domains as follows:

$$H^{(l)} = -\nabla\psi^{(l)}, l = 1, 2, 3 \quad (4)$$

Using Eqs. (2)–(4), the magnetic flux density $B^{(l)}$ in these sub-domains can be written in terms of the scalar potentials $\psi^{(l)}$ as:

$$B^{(l)} = -\mu_0(1 + \chi)\nabla\psi^{(l)}, l = 1, 2, 3 \quad (5)$$

The magnetic flux intensity (B) meets the principle of superposition. Assume the fluid is irrotational, then based on the principles of conservation of mass and momentum and the theories on magnetic fields, the perturbation part of the surface dynamic governing equations can be written as [19].

$$\nabla^2\psi = 0, -d \leq z \leq \zeta \quad (6)$$

$$\nabla^2\psi^{(l)} = 0, l = 1, 2, 3 \quad (7)$$

$$-\rho \frac{\partial \phi}{\partial t} + \rho g \zeta + \chi B_0 \frac{\partial \psi^{(2)}}{\partial z} - \sigma \left(\frac{\partial^{(2)} \zeta}{\partial r^{(2)}} + \frac{1}{r} \frac{\partial \zeta}{\partial r} + \frac{1}{r^{(2)}} \frac{\partial^{(2)} \zeta}{\partial \theta^{(2)}} \right) = 0, z = \zeta \quad (8)$$

where ρ is the density of the fluid, σ is the surface tension, φ , and $\psi^{(l)}$, $l = 1, 2, 3$ are the perturbation components of the fluid velocity potential and the magnetic potential, respectively. Using the following two boundary conditions:

$$-\frac{\partial\Phi}{\partial z} = \frac{\partial\zeta}{\partial t}, z = \zeta \quad (9)$$

$$-\frac{\partial\Phi}{\partial z} = 0, z = -d \quad (10)$$

The solutions concerning the input $\psi_{ij}(t)$ thus are obtained as follows:

$$\zeta(r_k, \theta_k, t) = \tilde{\zeta}_{ij}(t) J_m(\lambda r_k) \Theta(\theta_k) \quad (11)$$

$$\phi(r_k, \theta_k, z, t) = -\frac{1}{\lambda} \frac{\cosh[\lambda(z+d)]}{\sinh(\lambda d)} \frac{d\tilde{\zeta}_{ij}}{dt} J_m(\lambda r_k) \Theta(\theta_k) \quad (12)$$

$$\phi^{(2)}(r_k, \theta_k, z, t) = -\left[A_{ij}(t) \left(\frac{\mu}{\mu_0} \cosh \cosh(\lambda z) - \sinh \sinh(\lambda z) \right) + \frac{\chi}{\mu} B_0 \tilde{\zeta}_{ij}(t) \cosh(\lambda z) \right] J_m(\lambda r_k) \Theta(\theta_k) \quad (13)$$

where $J_m(\cdot)$ is the Bessel function of the first kind, λ is the separation constant, and

$$\Theta(\theta) = \{ \sin m\theta, m = 1, 2, 3 \dots \cos m\theta, m = 0, 1, 2, 3 \dots \} \quad (14)$$

$$A_{ij}(t) = \frac{1}{Y(-\lambda h_i)} \times \left\{ Z(-\lambda h_i) B_0 \tilde{\zeta}_{ij}(t) + \frac{\kappa}{\pi R^2 [J_{m+1}(\varepsilon)]^2} \psi_{ij}(t) R(r_{ij}) \Theta(\theta_{ij}) \right\} \quad (15)$$

$$Y(-\lambda h_i) = -\frac{1}{\tanh(\lambda d) - \coth(\lambda d)} \times \left\{ \frac{\mu}{\mu_0} (\alpha + \chi) \cosh \cosh(-\lambda h_i) - \left(\frac{\mu}{\mu_0} (\alpha - \chi) - \frac{\chi^2}{\alpha} \right) \sinh(-\lambda h_i) \right\} \quad (16)$$

$$Z(-\lambda h_i) = -\frac{1}{\tanh(\lambda d) - \coth(\lambda d)} \times \{ \alpha \cosh(-\lambda h_i) - \chi \sinh(-\lambda h_i) \} \frac{\chi}{\mu} \quad (17)$$

$$\alpha = \frac{\mu}{\mu_0} \tanh(\lambda d) - \coth(\lambda d), \kappa = \{ 1 \ m = 0 \ 2 \ m \neq 0 \}$$

Considering that the miniature coils are located far from the walls of the fluid container, so at $r = R$ yields $J_m(\lambda R) = 0$, which can be solved numerically and yields an infinite number of solutions $\varepsilon_{mn} = \lambda R$, $m = 0, 1, 2, \dots$, $n = 1, 2, 3, \dots$, providing the eigenvalue λ_{mn} for each mode as $\lambda_{mn} = \varepsilon_{mn}/R$. Combining $J_m(\lambda_r)$ and $\Theta(\theta)$, we define the following mode shapes as $H_{mnc} = J_m(\lambda_{mn} r) \cdot \cos(m\theta)$ and $H_{mns} = J_m(\lambda_{mn} r) \cdot \sin(m\theta)$.

For any coil $\psi_{ij}(t)$ on each layer, based on Eq. (8) and the damping effect associated with the fluid viscosity η , the following surface dynamic equation with respect to the mode shape H_{mnc} can then be obtained as:

$$\frac{d^2 \tilde{\zeta}_{ijmnc}(t)}{dt^2} + 4 \frac{\eta}{\rho} \lambda_{mn}^2 \frac{d \tilde{\zeta}_{ijmnc}(t)}{dt} - \omega_{imn}^2 \tilde{\zeta}_{ijmnc}(t) = -\frac{\chi}{\rho} B_0 \frac{\tanh(\lambda_{mn} d)}{Y(-\lambda_{mn} h_i)} \lambda_{mn}^2 \frac{\kappa}{\pi R^2 [J_{m+1}(\varepsilon_{mn})]^2} \psi_{ij}(t) H_{mnc}(r_{ij}, \theta_{ij}) \quad (18)$$

where

$$\omega_{imn}^2 = g \tanh(\lambda_{mn}d) \lambda_{mn} + \frac{\sigma}{\rho} \tanh(\lambda_{mn}d) \lambda_{mn}^3 + \frac{\chi}{\rho} B_0^2 \tanh(\lambda_{mn}d) \lambda_{mn}^2 \frac{Z(-\lambda_{mn}h_i)}{Y(-\lambda_{mn}h_i)} \quad (19)$$

$m = 0, 1, 2, \dots$ and $n = 1, 2, 3, \dots$

The main idea of the derivation of Eq. (18) is similar to the result of MFDM with a single-layer layout of actuators and more details can be found in [19]. A similar set of equations can be obtained concerning the mode shape H_{mns} as:

$$\begin{aligned} & \frac{d^2 \tilde{\zeta}_{ijmns}(t)}{dt^2} + 4 \frac{\eta}{\rho} \lambda_{mn}^2 \frac{d \tilde{\zeta}_{ijmns}(t)}{dt} - \omega_{imn}^2 \tilde{\zeta}_{ijmns}(t) \\ & = -\frac{\chi}{\rho} B_0 \frac{\tanh(\lambda_{mn}d)}{Y(-\lambda_{mn}h_i)} \lambda_{mn}^2 \frac{\kappa}{\pi R^2 [J_{m+1}(\epsilon_{mn})]^2} \psi_{ij}(t) H_{mns}(r_{ij}, \theta_{ij}) \end{aligned} \quad (20)$$

where m and $n = 1, 2, 3, \dots$

The generalized displacements $\tilde{\zeta}_{ijmnc}(t)$ and $\tilde{\zeta}_{ijmns}(t)$, obtained from the solution of the second-order differential Eqs. (18) and (19) respectively, and the corresponding mode shapes H_{mnc} and H_{mns} evaluated at any desired location (r_k, θ_k) , give the total surface displacement at the location as:

$$\begin{aligned} \zeta(r_k, \theta_k, t) &= \sum_{i=1}^2 \sum_{j=1}^{J_i} \sum_{m=0}^{\infty} \sum_{n=1}^{\infty} \tilde{\zeta}_{ijmnc}(t) H_{mnc}(r_k, \theta_k) \\ &+ \sum_{i=1}^2 \sum_{j=1}^{J_i} \sum_{m=0}^{\infty} \sum_{n=1}^{\infty} \tilde{\zeta}_{ijmns}(t) H_{mns}(r_k, \theta_k) \end{aligned} \quad (21)$$

Eqs. (18)–(19) show that the surface response $\zeta(r_k, \theta_k, t)$ has linear relation with the input $\psi_{ij}(t)$ applied by each coil. Note that the static surface response model of the mirror can be attained by the perturbed magnetic field of each actuator. For more details refer to Ref. [20].

This section introduced the current method to improve the correction performance of the MFDM for full-order aberrations, a new MFDM with a two-layer of actuators.

3. Nanoparticle manipulations for biomedical applications

The application of magnetic nanoparticles (NPs) has been extensively studied in biomedicine such as in imaging contrast enhancement [21] (see more detail in Section 4), magnetic separation [22], hyperthermia treatment [23], and targeted drug delivery [24] (see more detail in Section 5).

Due to their size, NPs can interact with biological systems at the molecular level and pass through biological barriers [24]. Using an external magnetic field to manipulate and to guide magnetic NPs to the wanted location has obtained special attention.

Several studies describe different magnetic nanoparticles as well as different delivery techniques [25]. Magnetite NPs (e.g., Fe_3O_4) are the most widely used due to several appealing properties [26]. This type of NPs exhibit superparamagnetism which means that they do not have magnetic moment when there is no external field but become magnetized when an external magnetic field is applied.

This property is of great value for a variety of biomedical applications as magnetite NPs do not form into a mass together and can move easily through blood vessels [26]. The typical shape of these NPs is a sphere with the size of around 5–100 nm. Most importantly, Fe_3O_4 NPs are biocompatible which makes it suitable for many biomedical applications [27].

Currently, one of the leading research interests is associated with the delivery of magnetic NPs to a target location. Several approaches have been proposed to address the issue. For example, the surface of magnetic NPs has been modified with biomolecules to identify and attach to target cells. Also, injection of magnetic NPs to some localized regions has been suggested [28]. Furthermore, using an external force to control the NPs in the desired direction remotely has been proposed [29]. When an electric current passes through the micro-coils, it generates a non-uniform magnetic field which attracts the NPs at its minimal. The magnitude of the magnetic field B relates to the size of the wire as $B \propto I/d$, gradients of the field as $\nabla B \propto I/d$ [22], and curvatures as $\nabla^2 B \propto I/d$ [23], where I is the electric current through the wire [30]. The magnetic gradient makes it possible to trap magnetic NPs within a micrometer and sub-micrometer regions using small coils. The focusing depth of the micro-coils is in the range of tens of microns to several millimeters. The fluid containing magnetic NPs is usually placed on the top of the device allowing for magnetic manipulation of NPs. Such a method has been shown in several works for trapping and positioning of magnetic NPs by different types of micro-electromagnets [29, 31]. This provides the possibility of controlling the strength of the field using external parameters such the current passing through micro-coils.

As an example, this method [32] is used for focusing and selective destruction of red blood cells (RBCs) via magnetic NPs. The experiment was accomplished above the micro-electromagnet serving concurrently as a source of the magnetic field and as a local heater. The motion and focusing of the blood cells near wires which carry the electric current were observed in the previous study. It was also found that the increase of the electric current through the micro-electromagnet leads to the local cell hemolysis. All the previous results have been obtained for the case when the guiding magnetic field was produced by just one conducting contour. In this work, experimental data was obtained for the modified micro-electromagnet with two contours, where the current in each path can be individually controlled. This modification gives an extra degree of freedom to tune the magnetic field profile and to manipulate magnetic nanoparticles.

The schematics of the micro-magnetic prototype with biological substance and the external electric circuit are shown in **Figure 4(A)**. The device is fabricated on the top of a fused silica substrate. It consists of two Cu wires fabricated by standard optical lithography techniques. The width of the wires is 10 μm , and the height of the wires is 2 μm . The minimum spacing between the wires is 20 μm . Each of the two wires has individual contacts (1 mm \times 1 mm) on the sides of the structure for connection with the outer electric circuit. The circuit includes a power source and two electrical relay switches allowing for the individual control of electric current in each wire. The wires are covered by a 300 nm thick layer of silicon dioxide deposited via PECVD which allows for both electrical insulations as well as corrosion protection for the Cu wires. The top part of the structure is the working area where the manipulation of biological cells takes place. As a test biological substance, human red blood cells (RBC) are obtained from fresh blood samples. RBC was selected both due to their availability as well as their robustness [33]. Samples were prepared by triple washing using centrifugation at 2000 rpm on an Eppendorf 5424 centrifuge in phosphate buffered saline solution (PBS) at room temperature. PBS was prepared from 10 \times PBS (Fisher Scientific, USA) concentrate solution with a final concentration of 2000–4000 cells/ μl . From this RBC solution, 30 μl of the

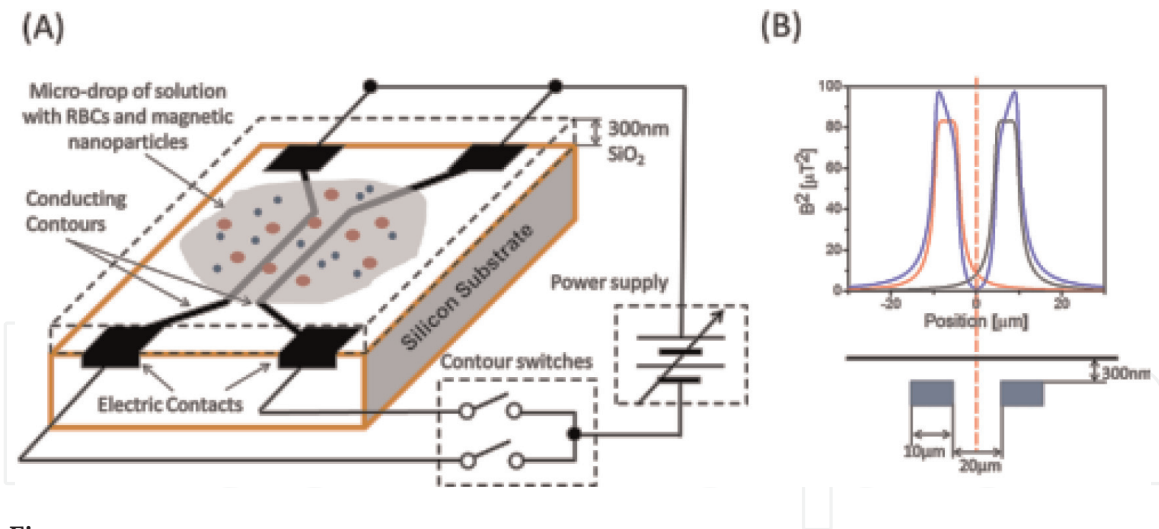


Figure 4. (A) Schematics of the micro-electromagnet and the external electric circuit. The device is fabricated on the top of a fused silica substrate. It consists of two Cu wires fabricated by optical lithography. The width of the wires is 10 μm , and the height of the wires is 2 μm . The wires are covered by the 300 nm of silicon dioxide. The top part of the structure is the working area where solution with biological cells and magnetic nanoparticles is placed. (B) Results of numerical modeling showing the surface profile of the scaled magnetic energy B^2 produced by the current-carrying wires. The red and the black curves show the scaled magnetic energy when 100 mA electric current is flowing through one of the contours. The blue curve shows the scaled magnetic energy when an electric current is flowing through both contours (adapted from [34]).

solution are then mixed with 1 μl of commercially available ferrofluid from Ferrotec containing 1.1% magnetite (Fe_3O_4) particles in aqueous solution.

The electric current passing through the wire generates a non-uniform magnetic field around it. The gradient of this non-uniform magnetic field causes the magnetic NPs to be attracted towards the wires. Therefore, the movement of magnetic NPs pulls biological cells in the same direction [32]. **Figure 4(B)** shows the numerical results of the magnetic energy above the two straight wires. The red and black curves show the magnetic energy when the current is 100 mA in one of the wires. The blue curve shows the magnetic energy when the current passes through both wires. There is an overlap between the magnetic fields in the region and the wires (as depicted by the red dashed line in **Figure 4(B)**). This overlap is important for sequential trapping of magnetic NPs by applying a current through one or the other wires. The maximum of the field gradient is about 1.4 mT/ μm in the vicinity of the current-carrying wire.

The individual control of electric current (hence magnetic field) in the two contours allows for a variety of experiments to be conducted on biological cell manipulation. This application shows that the biological cell manipulation is possible due to the presence of magnetic nanoparticles. To support this statement, some studies performed control experiments with RBC samples without adding magnetic nanoparticles [34]. It is shown that applying a magnetic field without nanoparticles initiates a slight motion of RBCs away from the field source which is attributed to local heating and the expanding solution. However, when the study is conducted by adding 1.1% magnetic nanoparticles, applying the magnetic field results in the cells focusing near the field source. The focusing is attributed to the drag effect, where a flow of magnetic nanoparticles drags the cells in the same direction. The potential application of this is that with time-varying magnetic field one can move RBCs towards or away from the specific region. This technique can be further evolved for precise controlling of cellular motion and drug-carrying cells. There are many questions related to the mechanism of magnetic nanoparticles interaction with living cells which deserve separate studies and it is out of the scope of this chapter. Nanoparticle manipulation using magnetic field potentially may be useful in various areas including molecular biology, medicine, gene engineering, and drug delivery technology.

4. Biomedical imaging contrast enhancement

MHD plays an important role in biomedical imaging, ranging from magnetic resonance imaging (MRI) that employs the endogenous magnetization contrast of water in tissue to magnetofluids acting as contrast agents in a number of imaging modalities. These contrast agents enhance the ability to detect tumors, infection, inflammation, infarction or lesions in the body. This section highlights the role of magnetic fluids as contrast enhancing agents in MRI, X-ray computed tomography (CT) and optical coherence tomography (OCT) imaging.

4.1 Contrast agents in MR imaging

MRI is one of the major biomedical applications of MHD. MRI is a non-invasive tomographic medical imaging technique based on nuclear magnetic resonance (NMR) that provides high-resolution images of soft anatomical structures such as brain, heart, ligaments, and eyes [35–41]. This information is vital in delineating healthy from diseased tissues or organs. MRI takes advantage of the inherent magnetic dipole moments of the atomic nuclei in our bodies, specifically hydrogen nuclei contained in water—that makes about 70% of our body mass. Three magnetic fields comprising of a static magnetic field (SMF), a time-varying gradient magnetic fields (GMF) and a pulsed radiofrequency field (RF) are used to probe the magnetization/demagnetization map of the body. The water molecules that occupies most of the tissue in the body consist of hydrogen atoms with nuclei that possesses a quantum-mechanical spin. The hydrogen nucleus spin is associated to a magnetic dipole moment (**Figure 5(A)**) that gets aligned to a strong magnetic field B_0 with a bulk magnetization M_{z0} along B_0 when the body is placed in it as shown in **Figure 5(B)**. Since these hydrogen nuclei dipoles have an angular momentum from the rotation about their own axes, they precess around the B_0 magnetic field axis with an angular frequency that follows Larmor equation $\omega = \gamma B_0$, where γ is the gyromagnetic ratio constant of the hydrogen nucleus. The precession gives rise to a transverse magnetic field that can be detected by a coil conveniently placed in the system to pick up this signal. The equation of the signal detected is proportional to $S(t) = \gamma B_0 \rho \sin(\theta) \sin(\omega t)$, here γ is the gyromagnetic ratio constant of the hydrogen nucleus, B_0 the magnetic field intensity of the static magnetic field, ρ the density of hydrogen nuclei of the tissue, θ the flip angle between the axis of the SMF and the

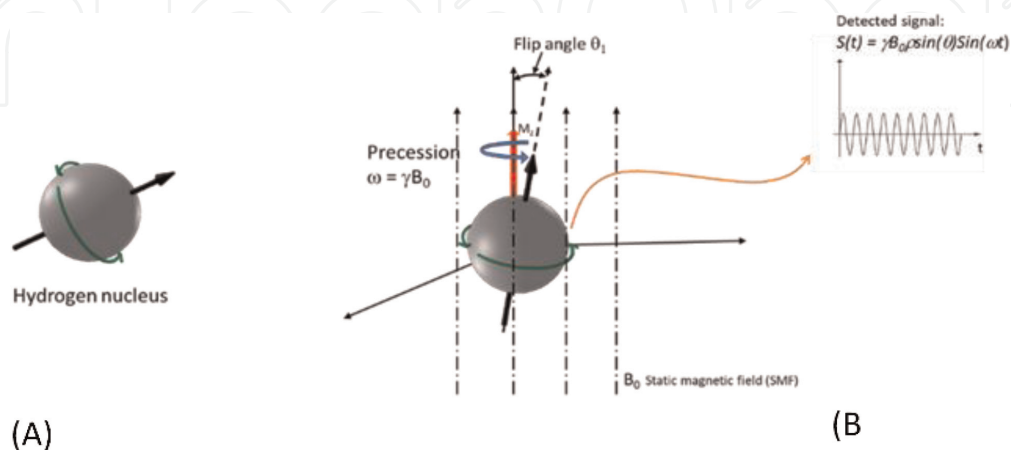


Figure 5.

(A) The hydrogen nucleus possesses a quantum-mechanical spin (angular momentum) that is associated with a magnetic dipole moment. (B) When the body is placed in a strong magnetic field B_0 , the hydrogen nuclei dipoles get aligned with the field B_0 with a net magnetization vector M_{z0} . The dipoles precess around the axis of the magnetic field with an angular frequency that follows Larmor equation $\omega = \gamma B_0$, where γ is the intrinsic gyromagnetic ratio constant of the hydrogen nucleus.

rotation axis of the hydrogen nucleus and ω the Larmor angular frequency. When a resonant pulsed RF magnetic field is applied perpendicular to the SMF, the hydrogen nuclei process around the SMF axis in phase. After removal of RF pulse, the spins begin to diphas and so the detected transverse magnetic field M_T signal starts to decrease. It does so according to the equation $M_T(t) = M_T(0) \exp\left(\frac{-t}{T_2}\right)$, where T_2 is called the spin-relaxation time. The nuclei return to their initial equilibrium state before the RF pulse by emitting an MR signal which also occurs by stimulation from surrounding nuclei. The process is assumed to occur in a simple exponential manner according to the equation $M_Z(t) - M_0 = (M_{Z0} - M_0) \left(1 - \exp\left(\frac{-t}{T_1}\right)\right)$, where T_1 , the time required for the nuclei system to return to 63% the equilibrium state, is called the spin-lattice relaxation time [42–44] (**Figure 6**).

Tissue/organ contrasts in MRI arises from differences in mainly these two basic physical parameters: the difference in the spin-relaxation time T_1 in the different organs required for the realignment to the SMF by the hydrogen nuclei of after the RF pulse is removed; the time constant T_2 with which the spins' signals arising from a given tissue will diphas after the pulsed RF signal is removed. **Figure 7** shows the variation in the longitudinal magnetization M_Z characterized by T_1 and the decay in

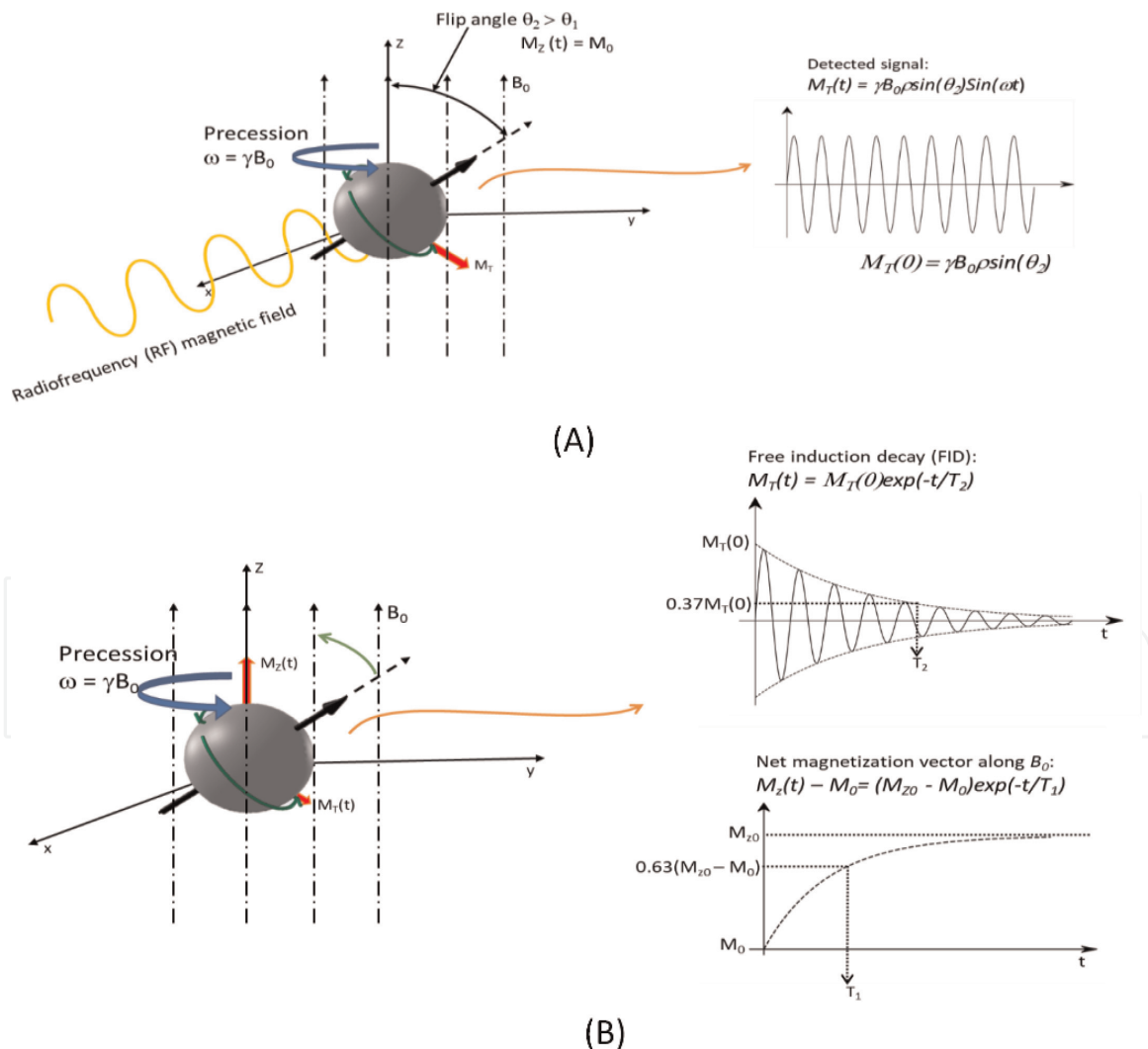


Figure 6. (A) When a 90° RF pulse is applied to the aligned magnetic dipoles, the net magnetization gets tipped to the transverse xy -plane. Dephasing of the spins results in a quick decrease of the net magnetization in the xy -plane M_T . The dephasing occurs exponentially and characterized by T_2 . (B) After the pulsed magnetic field is removed, the longitudinal magnetic field M_Z begins to grow exponentially to a maximum of M_{Z0} ; this growth is characterized by a parameter called T_1 , which the time it takes for the net magnetization along B_0 to grow to 63% of the maximum value M_{Z0} .

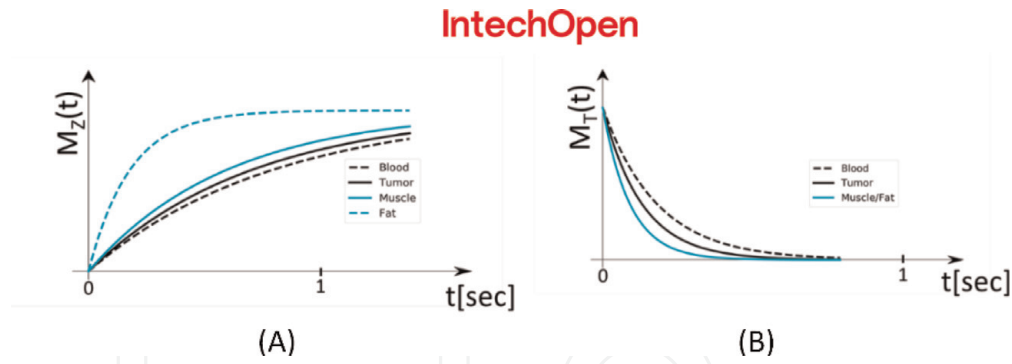


Figure 7. (A) The T_1 relaxation time, known as the spin-lattice relaxation time, is the measure of how fast the net magnetization vector (NMV) occurs along the SMF. Different tissue in the body possesses different T_1 relaxation times (a) which act as a contrast for the different tissue and even of diseased tissues such as tumors. (B) T_2 relaxation refers to the progressive dephasing of spinning dipoles following the 90° pulse as seen in a spin-echo sequence due to tissue-particular characteristics (b).

the transverse magnetization M_T , characterized by T_2 in the different tissues in the body [45].

Magnetic fluids play an important role as contrast enhancing agents in MRI. These contrast agents serve to shorten the relaxation time of the water molecules surrounding the tissue or organs with the contrast agent molecules, which then increases the signal intensity detected and thereby providing a positive contrast. The contrast agents used in MRI can broadly be divided into two major categories: the T_1 -weighted contrast agents and T_2 -weighted contrast agents. T_1 -weighted contrast agents shorten the T_1 relaxation time to improve the T_1 relaxation contrast, brightening the T_1 -weighted image. T_1 contrast agents usually consist of gadolinium (Gd) compounds. On the other hand, T_2 contrast agents serve to brighten the T_2 -weighted images by shortening the T_2 relaxation time. T_2 contrast agents consist mainly of superparamagnetic iron oxide and iron platinum. **Table 4** summarizes the major commercially available magnetic fluids used as contrast agents in MRI imaging today.

Compounds	Trade name	Target organs and tissue	Reference
<i>T₁-weighted contrast agents</i>			
Gadopentetate dimeglumine (Gd-DTPA)	Magnevist [®]	Glioma	[46, 47]
Gadoterate meglumine (Gd-DOTA)	Dotarem [®]	Brain and spine	[48]
Polyamidoamine	Dendrimer [®]	Angiography and tumor differentiation	[49]
Gadoxetate disodium (Gd-EOB-DTPA)	Primovist [®]	Liver	[50]
Gadodiamide (Gd-DTPA-BMA)	Omniscan [®]	Blood vessels	[51]
Gadobenate dimeglumine (Gd-BOPTA)	MultiHance [®]	Liver	[52]
Gadoteridol (GD-HP-DO3A)	ProHance [®]	Brain and spine	[53]
Gadoversetamide (C ₂₀ H ₃₄ GdN ₅ O ₁₀)	OptiMARK [®]	Brain, spine, and liver	[54]
Gadobutrol (Gd-BT-DO3A)	Gadovist [®] / Gdavist [®]	Angiography	[55]
Gadocoletic acid trisodium	Gadocoletic acid	Angiography	[56]

Compounds	Trade name	Target organs and tissue	Reference
Gadomelitol	Vistarem [®] (Gadomelitol)	Angiography	[57]
Gadoteric acid (Gd-DOTA)	Clariscan TM	Brain and spine	[58]
<i>T₂-weighted contrast agents</i>			
Ferumoxide (AMI-25) (Fe ₃ O ₄ ·γFe ₂ O ₃)	Feridex [®]	Liver, spleen, Bone marrow	[59, 60]
Ferumoxsil (AMI-121) (Fe ₃ O ₄ ·γFe ₂ O ₃)	Lumirem [®]	Liver, spleen, gastrointestinal tract	[61]
Ferumoxtran (Fe ₃ O ₄ ·γFe ₂ O ₃)	Sinerem [®]	Lymph nodes, blood	[62]
Ferrixan (Fe ₃ O ₄)	Resovist [®]	Liver	[63]

Table 4.
 Commonly used MRI contrast agents for medical diagnosis.

4.2 Contrast agents in X-ray and CT

Computed tomography (CT) is a powerful non-invasive diagnostic imaging technique [64]. CT can be employed for imaging hard organs or tissues (e.g., bones) or soft ones such as the gastrointestinal (GI) tract, the cardiovascular system, renal tract, liver, lungs, cartilage, and tumorous tissue with the aid of contrast agents. A CT image is obtained by rotating an X-ray source(s) (or detector/detector array) around an object or vice versa, with a detector(s) positioned directly opposite the radiation source(s). Generally, X-ray scans are taken at small angular increments during rotation around the object over 360° or 180° [65]. An X-ray attenuation (or phase or scattering) map or projections are thus obtained. The projections are then processed mathematically to create a 3D rendering of the scanned object.

Another diagnostic imaging method related to CT is X-ray fluoroscopy—form of a projection imaging with contrast agent. Fluoroscopy allows for the acquisition of real-time, continuous images of the internal organs. Like in MRI, imaging contrast agents are often used in X-ray imaging for better contrast resolution. Usually, small iodinated agents are injected into blood vessels for use in fluoroscopic angiography, allowing for the evaluation of blood flow and visualization of the vasculature system, while barium contrast media are introduced orally or with an enema to investigate the anatomy (and pathology) of the gastrointestinal tract. The X-ray absorption coefficient μ can be expressed as:

$$\mu \approx \frac{\rho Z^4}{AE^3} \quad (22)$$

where ρ is the density of the material, Z the atomic number, A the atomic mass and E the X-ray energy. Therefore, materials of higher density and atomic number, higher density tissues, absorb X-ray better [66].

While lanthanide-based contrast agents are a common stay in MRI, their application in CT as contrast agents is being explored based on their high atomic numbers [64]. The two major reasons motivating the investigation of gadolinium-based compounds as CT contrast agents include use in patients who are contraindicated for iodinated agents based on allergic reactions or renal insufficiency and the fact that *Gd* has higher K edges than iodine providing better contrast enhancement at higher X-ray photon energies, potentially reducing radiation exposure to patients [67]. A summary of some of the gadolinium compounds used in MRI as contrast agents are listed in **Table 4**. Clinically approved gadolinium-based contrast agents

Compound	Trade name	Target organ	Reference
1. Gadopentate dimeglumine (Gd-DTPA)	Magnevist [®]	Urinary tract, aorta, blood vessels in cranium	[68, 69]
2. Gadodiamide (Gd-DTPA-BMA)	Omniscan [®]	Arterial angiography,	[70]
3. Gadoteridol (Gd-HP-DO3A)	ProHance [®]	Aorta, brain tumors,	[71]
4. Gadobutrol (Gd-BT-DO3A)	Gadovist [®]	Alternative to iodinated agents	[72]
5. Gadoxetate disodium (Gd-EOB-DTPA)	Primovist [®]	Liver, spleen, urinary tract	[73]

Table 5.
Lanthanide-based contrast agents for CT and X-ray.

have been tested in CT for imaging the cardiovascular system and for pulmonary and aortic angiography. **Table 5** summarizes some of the *Gd* compounds that have been tested as contrast agents in CT.

4.3 Magnetic contrast agents in OCT imaging

OCT is non-invasive cross-sectional imaging modality that uses light to interrogate tissue providing a 3D rendering of the tissue under investigation [74]. **Figure 8** depicts the principle of OCT. A low-coherence light from a laser source is split into two halves, with one half guided to a mirror (reference arm) and the other half used to illuminate the tissue under investigation (sample arm). The reflections from the reference arm and from the tissue are recombined by beam combiner and detected. The electrical signal from the photodetector is bandpass digitized and demodulated before being stored on a computer. The low-coherence in the light being used allows for interference between the two arms to occur only when the two optical path lengths are equal. Therefore, fine scanning of the reference arm mirror allows for interference to occur with light originating from the different depths of the tissue. Transverse scanning of the optical beam then allows for a 3D imaging of the tissue [75].

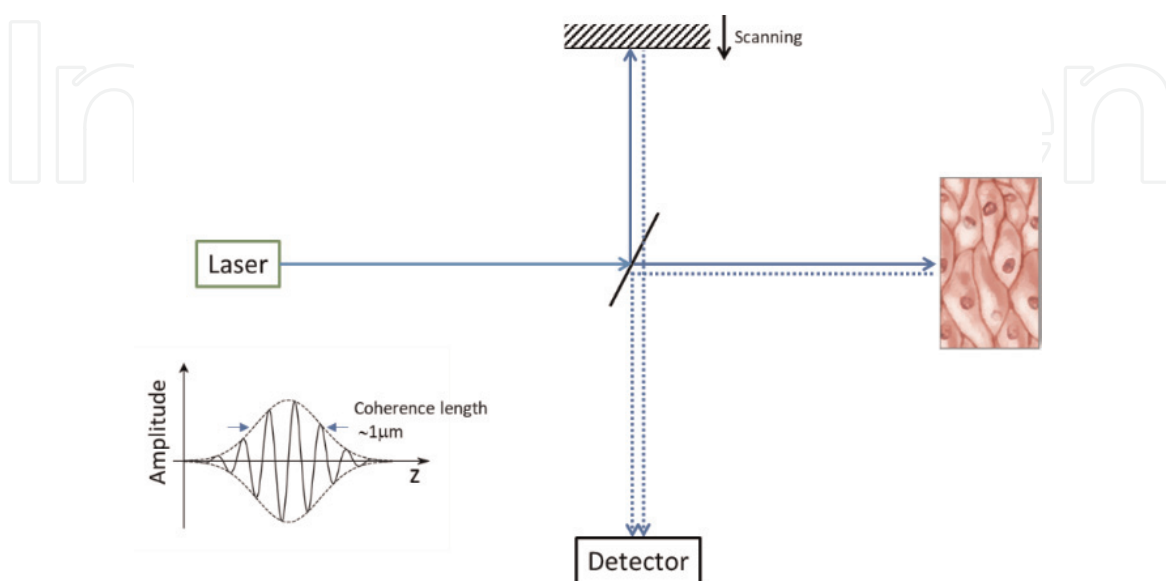


Figure 8.
Schematic illustrating the concept of low coherence interferometry. Using a short coherence length light source and a Michelson-type interferometer, interference fringes are observed only when the path lengths of the two interferometer arms are matched to within the coherence length (l_c) of the light source (adapted from [41]).

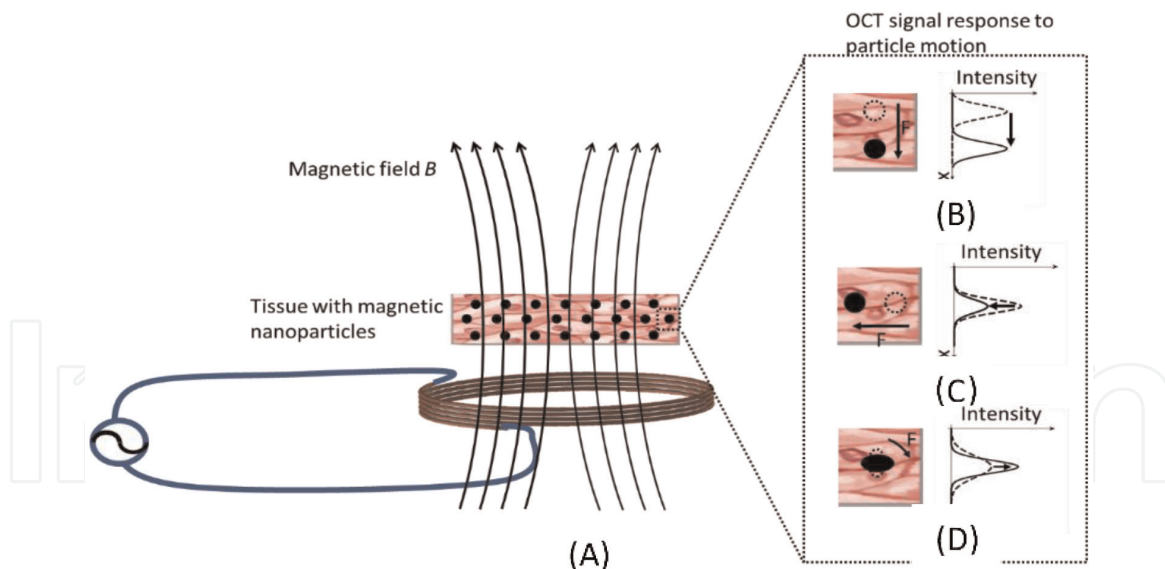


Figure 9. Magnetomotive OCT tissue configuration. (A) A sample is doped with magnetic microparticles, placed in a magnetic field and shone with an optical imaging beam. The contrast mechanisms illustrated by two states of a magnetic microparticle (filled and dash-outlined shapes, respectively) within the imaging focal volume and the associated (A–D).

The ability of a tissue to be magnetized is quantified as magnetic susceptibility χ and can be used as means of contrast in OCT imaging. Biological tissue is comparatively non-magnetic ($|\chi| \sim 10^{-5}$) when compared to ferromagnetic iron oxides, whose χ is 10^5 times greater than that of tissue. This means that the χ difference between tissue and magnetic particles can be exploited to provide contrast in OCT imaging of tissue doped with magnetic nanoparticles whose localized exogenously induced motion can be resolved by OCT and used as a contrast feature [76]. The motion of the nanoparticles in the tissue is caused by a magnetic gradient force:

$$\vec{F} = \frac{V(\chi - \chi_{med})\nabla|\vec{B}|^2}{2\mu_0} \quad (23)$$

where F is the force acting on the magnetic nanoparticles with susceptibility of χ within its surrounding tissue medium with susceptibility of χ_{med} , B being the magnetic flux density, V is the volume of the tissue nanoparticles and magnetic permeability in vacuum [77].

As shown in **Figure 9**, when the magnetic nanoparticles get laterally displaced by the magnetic force, the OCT the increase in the light scattered back also gets shifted laterally. **Figure 9(B–D)** shows the variation in the OCT signal variation that follow changes in the nanoparticles position arising from the magnetic force.

5. Targeted drug delivery

5.1 Introduction

As it was initially assumed by Widder et al. in 1978 [78], magnetic constructs can target specific locations, such as tumor sites, holding enormous potential for site-specific drug delivery, see **Figure 10**. This subchapter discusses a clinically driven application of MHD focusing on magnetic drug targeting. MHD drug targeting refers to the magnetically targeted and/or triggered therapeutic agent delivery

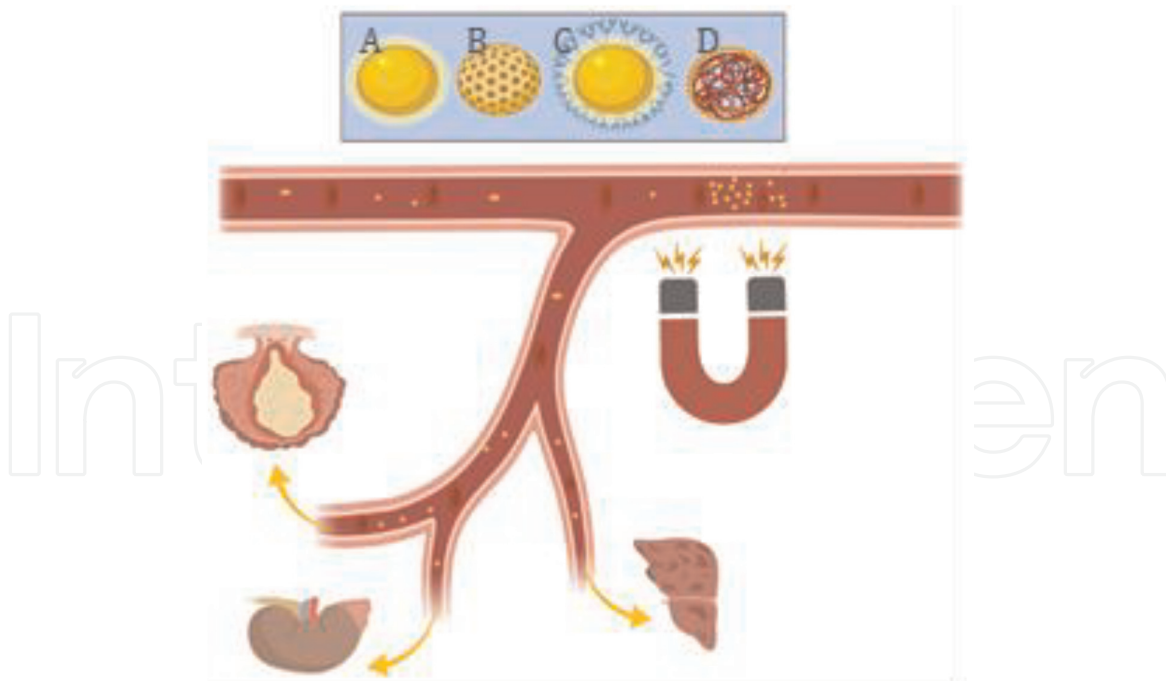


Figure 10.

Magnetic constructs (A) or constructs with evenly distributed magnetic material (B) applied parenterally (intravenously or intra-arterially), can be used as intravascular vehicles for targeted drug delivery if drug-loaded (C) or -coated (D).

method that augments the concentration of the agent in the target area. In the first part, drug-loaded magnetic constructs are discussed as individual intra-vascular vehicles for site-specific drug delivery. In the second part, magnetohydrodynamic (micro) pumps for controlling magnetic nanoparticles dispersed in a base fluid are discussed. These are reviewed and summarized separately based on the knowledge already available in literature.

5.2 Magnetic constructs

Due to their superior properties such as biocompatibility, biodegradability, large loading capacity, and controlled release ability, magnetic constructs have attracted a lot of attention. They offer mean to remotely direct therapeutic agents to well-localized sites of interest, improving control on dosing, reducing the concentration requirements up to 20% [79], associated toxicity, and fluctuation in circulating drug levels [80–82]. While drug release usually occurs by passive diffusion, triggering via enzymatic activity, physiological conditions [83] or magnetically [84–86], see **Figure 11**, can be performed. On-site controlled drug release is another important factor for effective therapeutics. For example, when the magnetic construct is exposed to an alternating magnetic field, drug release can occur. Via facilitated drug release, collateral tissue damage and toxic side effects may be further decreased or fully eliminated [87, 88]. This is important for applications balancing between efficacy and toxicity, e.g., chemotherapies [89].

The use of magnetic constructs as therapeutic agents has increased exponentially since the earliest studies by Senyei et al. [90] and magnetic carriers of increased sophistication have been developed [91]. While nanoparticles are the simplest magnetic constructs, currently, there are many different types of carriers for magnetic targeting. Generally, any biocompatible magnetic materials, magnetic materials coated by a biocompatible polymer or inorganic material, or magnetic materials precipitated inside the pores of a biocompatible polymer or inorganic material can be used. While the use of iron oxide particles in the form of magnetite (Fe_3O_4) or maghemite ($\gamma\text{-Fe}_2\text{O}_3$) predominates, any metal, e.g., cobalt or nickel, or

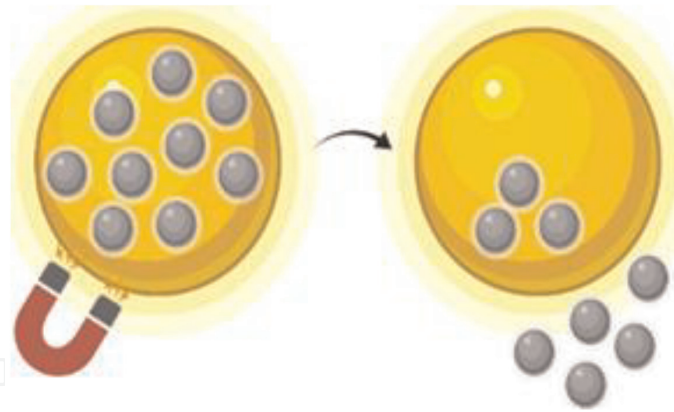


Figure 11.
 Targeted drug release.

metal derivatives, e.g., μ -oxo N,N'-bis(salicylidene)ethylenediamine iron-Fe(salen) [92–94], are used. Magnetic constructs can be porous or hollow single magnetic nano/microparticles encapsulating the drug in pores and cavities [95], non-magnetic polymeric or inorganic nano/microparticles encapsulating both magnetic material and drug [96], magnetosomes [97], micelles [98] or liposomes, micro/nanoswimmers or micro/nanomotors prepared by layer-by-layer deposition [99] or 3D-printing [100], nanoparticle clusters [96, 101].

The basic principle of magnetically targeted drug delivery is based on the physical phenomenon of the translational motion of a magnetic construct when a magnetic field gradient is applied. Magnetic construct with a therapeutic agent encapsulated into the construct and/or conjugated on its surface is injected systemically (or delivered locally via catheter) and transported by the blood circulation to the target location. While intravenous injection is associated with higher clearance from the bloodstream, it is being used more frequently when compared to the intra-arterial routes. A strong, high-gradient magnetic field is then applied to allow translating magnetic constructs to the target location and capturing them. Literature suggests that flux density at the target location must be of the order of a few hundred millitesla with a few teslas per meter field gradient for slow blood flow arteries and up to a few hundred for fast blood flow arteries.

Magnetic constructs are driven by the magnetic force F_m dependent on the magnetic induction B :

$$B = \mu_0(H + M) = \mu_0 H \quad (24)$$

where μ_0 is a permeability of free space, H is a magnetic field strength and M is a total magnetization of the magnetic construct which could be neglected in case of diluted suspension.

In the case of supermagnetic constructs in a diamagnetic base solution, the magnetic moment m on a magnetic construct:

$$m = V_m M = V_m \Delta\chi H = V_m (\chi_m - \chi_w) H \quad (25)$$

where V_m is a volume magnetic construct, $\Delta\chi$ is an effective susceptibility given via a difference between susceptibility of a magnetic construct χ_m and susceptibility of a base solution χ_w .

Under the assumption that magnetic constructs are very small and could be assumed to be point-like particles:

$$F_m = (m \cdot \nabla) B = \frac{V_m \Delta\chi}{\mu_0} (B \cdot \nabla) B = V_m \Delta\chi \nabla \left(\frac{B^2}{2\mu_0} \right) = V_m \Delta\chi \nabla \left(\frac{1}{2} B \cdot H \right) \quad (26)$$

On the one side, the magnetic force F_m depends on the magnetic constructs size (amount of magnetic material). While magnetic constructs are flexible in their dimensions from a few nanometers up to a few micrometers, there is a trade-off between larger magnetic force and the appropriate physiological response [82, 102, 103]. On the other side, the magnetic force is proportional to the magnetic gradient. The magnetization of the magnetic constructs, however, increases with the external magnetic field only while the magnetic field is below the saturation field.

In order to increase magnetic force up to several orders of magnitude further, magnetizable implant (biocompatible wire, needle, stent, filament or seed) creating a high-gradient magnetic field at the target location under the influence of an external magnetic field could be used, see **Figure 12** [104]. While implant can solve problem of magnetic force strength and distance decay, as well as being successfully used at MRI facilities in applications related to cardiovascular, digestive and urinary systems under clinically feasible conditions, it makes the procedure of magnetic drug targeting minimally invasive. The concept has been successfully demonstrated *in vivo* [105] and is promising for magnetically targeted thrombolytic therapy.

Although magnetic drug targeting is appealing, most studies demonstrate only *in vitro* results for superficial organs due to difficulties in manipulating magnetic particles *in vivo* and rapid decrease of magnetic force with distance [79]. While some technical challenges remain, several drug delivery systems have been developed for the treatment of pulmonary disorders [106, 107], cancer [108–110], and cardiovascular diseases [111].

5.3 MHD (micro)pumps

The concept of MHD (micro)pump is relatively new and was developed by Jang and Lee [112] only in 1999 with an initial goal of applying in drug delivery applications. The working fluid of MHD (micro)pump is magnetic fluids. The term nanofluid was previously introduced by Choi and Eastman [113] in 1995 and describes colloidal suspensions of magnetic nanoparticles or nanotubes ($d_\phi < 100$ nm) in a based solution e.g., water, oil, ethylene glycol mixture etc. Magnetic fluids, also called ferro- or nano-fluids, simultaneously exhibit liquid and magnetic properties, leading to the possibility to control their flows with magnetic fields.

In a typical setup, see **Figure 13**, a uniform magnetic field of strength B creates a controllable force (Lorentz force) F as a driving source in the flow for control and manipulation [114–119]. MHD (micro)pump can be fully described by a combination of Navier–Stokes equations of fluid dynamics and Maxwell’s equations of electromagnetism. Considering the absence of moving parts, MHD (micro)pump

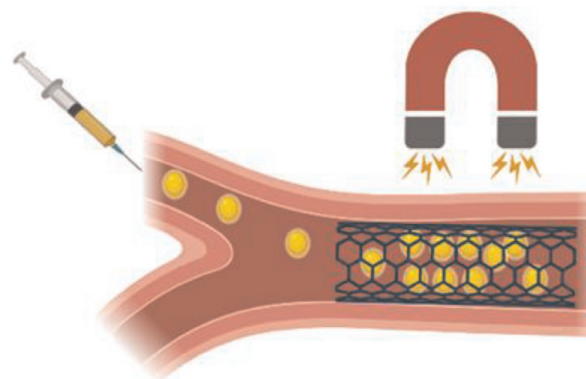


Figure 12.
Implant-assisted magnetic drug targeting with the magnetic stent implanted in the vasculature.

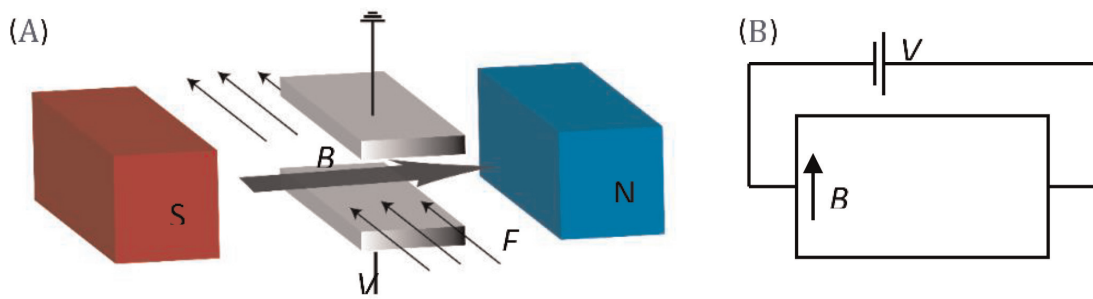


Figure 13. Schematic of MHD (micro)pump (A) and its simplification (B). When an electric potential difference V is applied between the electrodes, an electric current circulates through the electrically conducting magnetic fluid perpendicularly to the uniform magnetic field of strength B so that driving Lorentz force F is produced.

possess a simpler fabrication process when compared to mechanical (micro)pumps [120]. MHD (micro)pumps have attracted the attention of many researchers as they could achieve high flow rates and produce bi-directional flow. To use MHD (micro)pumps for drug delivery, however, the stability of the flow rate is critical. The flow rate of MHD (micro)pumps depends on the current and the magnetic flux density [112]. Nevertheless the flux density from a permanent magnet is higher than that of an electromagnet, some authors hypothesized that electromagnets are more useful as their polarity could be reversed, leading to the change of the flow direction [82]. The use of direct current (DC) and alternate current (AC) MHD (micro)pumps have been demonstrated [120]. While the application of direct current (DC) (micro)pumps is often associated with bubbles leading to electrode corrosion, they can achieve higher flow rates (Figures 14 and 15).

5.4 Magnetic separation via particle labeling

Magnetic separation is being used in many biomedical applications, particularly cellular separation [121]. It is achieved via labeling the desired biological entity, e.g., red blood cells, with biocompatible magnetic nanoparticles. Labeled objects are separated from the base solution by passing the mixture through a high magnetic field gradient immobilizing the labeled entities via the magnetic force:

$$F_m = 6\pi\eta R_m \Delta v \quad (27)$$

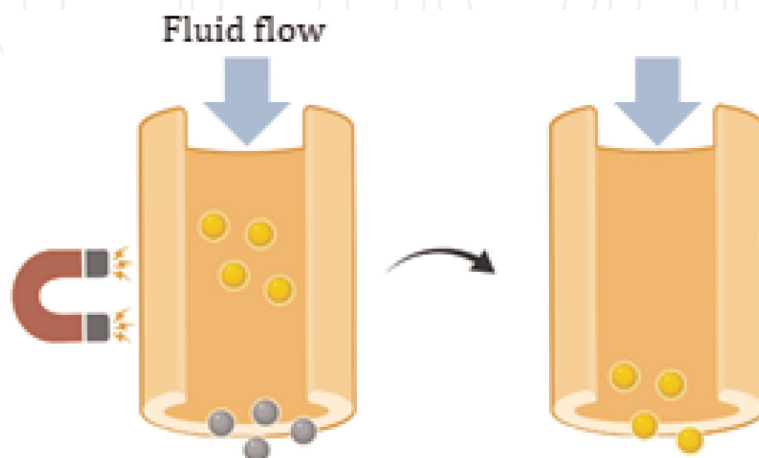


Figure 14. Magnetic separation. Left: while magnetically labeled objects (yellow) are attracted by the magnet, non-magnetic objects (gray) and base fluid can be filtered out. Right: after removing the magnetic force captured objects are recovered.

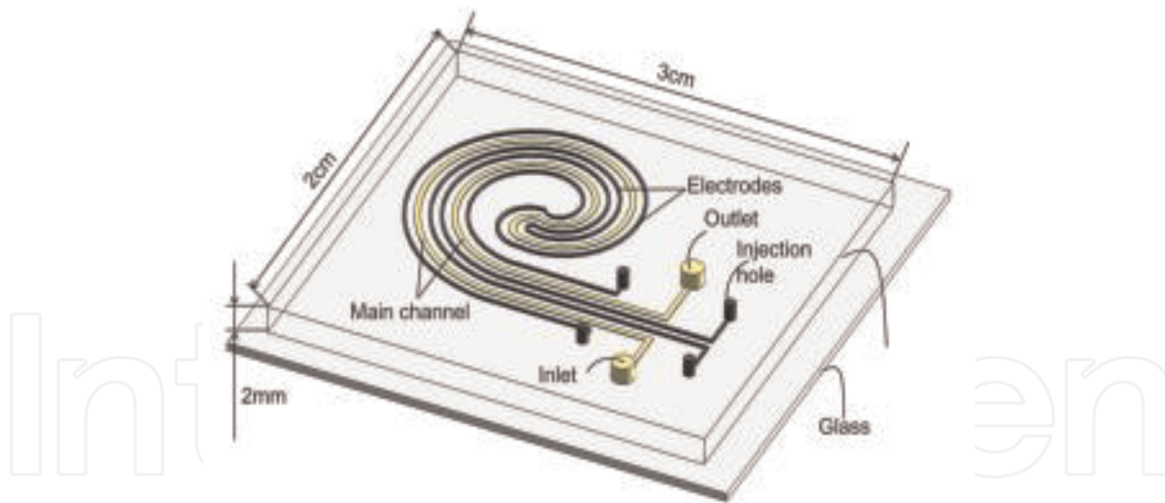


Figure 15.

Schematic of the polydimethylsiloxane (PDMS)-glass microfluidic chip for the liquid-metal-based magnetohydrodynamic (MHD) micropump (adapted from [122]).

where η is a base solution viscosity, R_m is a radius of magnetic nanoparticle, Δv is a relative velocity of nanoparticle with respect to the base solution.

6. Current biomedical devices based on magnetohydrodynamics

In this section, we describe some of the applications of MHD such as pumps, integrated fluidic networks, stirrer, and micro-coolers.

6.1 MHD-based micro-pumps

One of the best-known applications of MHD is in the field of fluid pumping. The device consists of a conduit with two electrodes on either side. When a potential difference is applied across the electrodes, current flux J flows through the solution. In the presence of a magnetic field B , the electric field J interacts with the magnetic field B to generate a Lorentz force $J \times B$ which drives fluid motion.

Below is an example of MHD-based micro-pumped on PDMS platform.

6.2 MHD-based microfluidic networks

In lab-on-chip applications, it is often necessary to transport fluids and reagents across networks of conduits. Controlling the flow usually requires the use of pumps and valves. It is hard to implement mechanical pumps and valve in a lab-on-chip setting. MHD provides a proper solution that does not require a mechanical component. The basic idea is to equip many of the network's conduits, if not all, with individually controlled electrodes. By careful control of the electrode's currents and in the presence of a magnetic field, it is possible to direct the fluid flow along any desired direction [123, 124].

Figure 16 shows a simple example of an MDH microfluidic network fabricated using low temperature co-fired ceramic tapes (LTCT). By programming, electrodes can circulate the fluid around the tours at any desired direction and even maintain their temperature allowing for various biological processes like thermal cycling and potentially polymerase chain reaction (PCR) for DNA amplification.

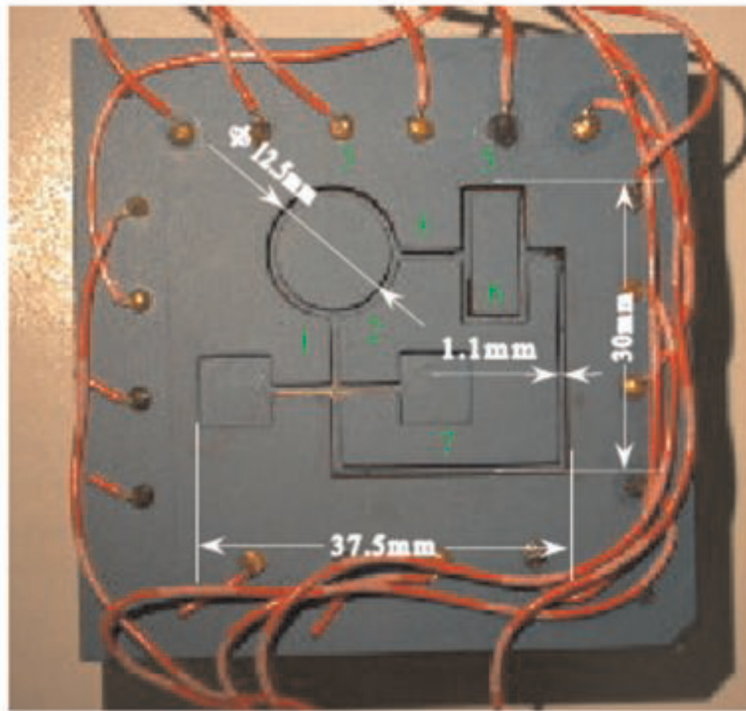


Figure 16.
A prototype of an MHD microfluidic network. The conduits are labeled with numbers (adapted from [125]).

6.3 MHD-based stirrer

Although the characteristic lengths associated with the microfluidic devices are small (e.g., in the order of $100\ \mu\text{m}$), diffusion alone does not allow sufficiently fast mixing. For example, at room temperature, myosin's diffusion coefficient in water is about $10^{-11}\ \text{m}^2/\text{s}$, and the diffusion time along with a length of $100\ \mu\text{m}$ is very large, about $10^3\ \text{s}$. Since Reynolds number (Re) of flows in micro-devices are usually very small ($Re \ll 1$), the flows are laminar, well-organized which cause poor mixing.

MHD provides us with rather easy means for mixing and stirring. Two different types of MHD stirrers have been reported in the literature. One relies on altering the flow direction to enhance dispersion [126, 127], while another type induces secondary flows to improve the mixing. For more details, refer to [126, 127].

In the current studies, it is shown that MHD is very suitable for providing better stirring in the microfluidic setting.

6.4 MHD-based micro-coolers

Since MHD can facilitate fluid circulation, it can be used to facilitate cooling. Liquid metals are particularly suitable for this purpose due to their high thermal conductivity, high boiling point temperature, and large electric conductivity. Since MHD propulsion is easy to implement, miniaturize and does not require mechanical components, it is ideal for micro-cooling applications, such as those required in microelectronics. Although various patents address MHD micro-coolers, it is not known whether any products are in actual use.

7. Conclusions

In summary, this chapter covers important aspects of the MHD applied in the biomedical field. A new MFDM with the two-layer layout is proposed to improve

the correction performance of the DM for full-order aberrations. The results showed the effectiveness of the method to correct full-order aberrations for adaptive optics systems. Furthermore, RBC manipulation by the magnetic field is demonstrated via an external magnetic field produced by a system of two current-carrying wires. It is shown that cell motion towards and away from the wires, as well as periodic motion in the region between the wires. This approach will likely have application in various fields including molecular biology, medicine, gene engineering, and drug delivery technology.

MHD plays an integral part in biomedical imaging, ranging from the endogenous magnetization properties of tissue that play an important role in MRI imaging to the ferromagnetic/superparamagnetic fluids that act as contrast enhancing agent in several imaging techniques such as MTI, CT/X-ray and OCT imaging. Several commercial contrast agents are in clinical use today. Research continues to be undertaken on new contrast agents and on the utility of MRI contrast agents in areas such as CT/X-ray and OCT imaging.

Moreover, the same magnetic constructs allow for a combination of enhanced diagnostic imaging (MRI, CT, OCT) and therapeutics (targeted drug delivery). While some technical challenges remain, several drug delivery systems have been successfully developed for treatment of pulmonary disorders, cancer, and cardiovascular diseases. At the end, we briefed current MHD-based devices with potential biomedical applications. MHD-based microfluidics operates at low voltages, can direct the liquid to flow along any desired path without a need for valves and pumps, and continuously circulate the sample in a closed loop, and furthermore can chaotically stir the sample without moving part.

Conflict of interest

Authors do not have a conflict of interest.

IntechOpen

Author details

Hamid Farrokhi*, David O. Otuya, Anna Khimchenko and Jing Dong
Wellman Center for Photomedicine, Massachusetts General Hospital and Harvard
Medical School, Boston, Massachusetts, USA

*Address all correspondence to: hfarrokhi@mgh.harvard.edu

IntechOpen

© 2019 The Author(s). Licensee IntechOpen. This chapter is distributed under the terms of the Creative Commons Attribution License (<http://creativecommons.org/licenses/by/3.0>), which permits unrestricted use, distribution, and reproduction in any medium, provided the original work is properly cited. 

References

- [1] Priest ER. *Solar Magnetohydrodynamics*. Cambridge, UK: Cambridge University Press; 2003
- [2] Freidberg JP. *Ideal Magnetohydrodynamics*. New York, NY: Plenum Press; 1987
- [3] Laughlin DR. A magnetohydrodynamic angular motion sensor for anthropomorphic test device instrumentation. SAE Technical Paper. 1989:892428
- [4] Jang J, Lee SS. Theoretical and experimental study of MHD (magnetohydrodynamic) micropump. *Sensors and Actuators A: Physical*. 2000;**80**:84-89
- [5] Lemoff AV, Lee AP. An AC magnetohydrodynamic micropump. *Sensors and Actuators B: Chemical*. 2000;**63**:178-185
- [6] Louis J, Lothrop J, Brogan T. Fluid dynamic studies with a magnetohydrodynamic generator. *Physics of Fluids (1958-1988)*. 1964;**7**:362-374
- [7] Rosa RJ. Physical principles of magnetohydrodynamic power generation. *Physics of Fluids (1958-1988)*. 1961;**4**:182-194
- [8] Lei X, Wang S, Yan H, Liu WJ, Dong LZ, Yang P, et al. Double-deformable-mirror adaptive optics system for laser beam cleanup using blind optimization. *Optics Express*. 2012;**20**:22143-22157
- [9] Sun B, Salter PS, Booth MJ. Pulse front adaptive optics: A new method for control of ultrashort laser pulses. *Optics Express*. 2015;**23**:19348-19357
- [10] Carroll J, Kay DB, Scoles D. Adaptive optics retinal imaging—Clinical opportunities and challenges. *Current Eye Research*. 2013;**38**:709-721
- [11] Sheehy CK, Tiruveedhula P, Sabesan R, Roorda A. Active eye-tracking for an adaptive optics scanning laser ophthalmoscope. *Biomedical Optics Express*. 2015;**6**:2412-2423
- [12] Merino D, Loza-Alvarez P. Adaptive optics scanning laser ophthalmoscope imaging: Technology update. *Journal of Clinical Ophthalmology*. 2016;**10**:743-755
- [13] Iqbal A, Amara FB. Modeling and experimental evaluation of a circular magnetic-fluid deformable mirror. *International Journal of Optomechatronics*. 2008;**2**:126-143
- [14] Parent J, Borra EF, Brousseau D, Ritcey AM, Déry JP, Thibault S. Dynamic response of ferrofluidic deformable mirrors. *Applied Optics*. 2009;**48**:1-6
- [15] Wu ZZ, Yuan S, Xie SR, Min LK, Huang MS. Response of magnetic fluid deformable mirror with large stroke surface deflection. *Magnetohydrodynamics*. 2015;**51**:695-708
- [16] Caprari RS. Optimal current loop systems for producing uniform magnetic fields. *Measurement Science and Technology*. 1995;**6**:593-597
- [17] Ritcey AM, Borra E. Magnetically deformable liquid mirrors from surface films of silver nanoparticles. *Chemphyschem*. 2010;**11**:981-986
- [18] Yen YT, Lu TY, Lee YC, Yu CC, Tsai YC, Tseng YC, et al. Highly reflective liquid mirrors: Exploring the effects of localized surface plasmon resonance and the arrangement of nanoparticles on metal liquid-like films. *ACS Applied Materials & Interfaces*. 2014;**6**:4292-4300
- [19] Wu ZZ, Iqbal A, Amara FB. Modeling and Control of Magnetic Fluid

Deformable Mirrors for Adaptive Optics Systems. Berlin, Germany: Springer; 2013

[20] Wu Z, Kong X, Zhang Z, Wu J, Wang T, Liu M. Magnetic fluid deformable mirrors with two-layer layout of actuators. *Micromachines*. 2017;**8**(3):72

[21] Josephson L. Magnetic nanoparticles for MR imaging. *BioMEMS and Biomedical Nanotechnology*. 2006: 227-237

[22] Morisada S, Miyata N, Iwahori K. Immunomagnetic separation of scum-forming bacteria using a polyclonal antibody that recognizes mycolic acids. *Journal of Microbiological Methods*. 2002;**51**:141

[23] Hergt R, Dutz S, Muller R, Zeisberger M. Magnetic particle hyperthermia: Nanoparticle magnetism and materials development for cancer therapy. *Journal of Physics: Condensed Matter*. 2006;**18**:S2919

[24] Kim T, Hyeon T. Applications of inorganic nanoparticles as therapeutic agents. *Nanotechnology*. 2014;**25**(1): 012001

[25] Rand RW, Snow HD, Elliott DG, Snyder M. Thermomagnetic surgery for cancer. *Applied Biochemistry and Biotechnology*. 1981;**6**:265

[26] Wahajuddin, Arora S. Superparamagnetic iron oxide nanoparticles: Magnetic nanoplateforms as drug carriers. *International Journal of Nanomedicine*. 2012;**7**:3445

[27] Moroz P, Jones SK, Gray BN. Magnetically mediated hyperthermia: Current status and future directions. *International Journal of Hyperthermia*. 2002;**18**(4):267

[28] Nagesha D, Devalapally H, Sridhar S, Amiji MM. Multifunctional

magnetic nanosystems for tumor imaging, targeted delivery, and thermal medicine. *Fundamental Biomedical Technologies*. 2008;**4**:381

[29] Lee CS, Lee H, Westervelt RM. Multifunctional magnetic nanosystems for tumor imaging, targeted delivery, and thermal medicine. *Applied Physics Letters*. 2001;**79**(20):3308

[30] Drndic M, Johnson KS, Thywissen JH, Prentiss M, Westervelt RM. Micro-electromagnets for atom manipulation. *Applied Physics Letters*. 1998;**72**:2906

[31] Lee H, Purdon AM, Chu V, Westervelt RM. Controlled assembly of magnetic nanoparticles from magnetotactic bacteria using microelectromagnets arrays. *Nano Letters*. 2004;**5**:995

[32] Gertz F, Azimov R, Khitun A. Biological cell positioning and spatially selective destruction via magnetic nanoparticles. *Applied Physics Letters*. 2012;**101**(1):013701

[33] Lovelock JE. The haemolysis of human red blood-cells by freezing and thawing. *Biochimica Et Biophysica Acta*. 1953;**10**:414

[34] Gertz F, Khitun A. Biological cell manipulation by magnetic nanoparticles. *AIP Advances*. 2016;**6**: 025308

[35] Hawkes RC, Holland GN, Moore WS, Worthington BS. Nuclear magnetic resonance (NMR) tomography of the brain: A preliminary clinical assessment with demonstration of pathology. *Journal of Computer Assisted Tomography*. 1980;**4**(5): 577-586

[36] Smith FW, Hutchison JM, Mallard JR, et al. Oesophageal carcinoma demonstrated by whole-body nuclear magnetic resonance imaging.

British Medical Journal (Clinical Research Ed.). 1981;**282**(6263):510-512

[37] Ogawa S, Lee T-M, Kay AR, Tank DW. Brain magnetic resonance imaging with contrast dependent on blood oxygenation. Proceedings of the National Academy of Sciences. 1990;**87**: 9868-9872

[38] Selskog P, Heiberg E, Ebbers T, Wigstrom L, Karlsson M. Kinematics of the heart: Strain-rate imaging from time-resolved three-dimensional phase contrast MRI. IEEE Transactions on Medical Imaging. 2002;**21**: 1105-1109

[39] Kupersmith MJ, Alban T, Zeiffer B, Lefton D. Contrast-enhanced MRI in acute optic neuritis: Relationship to visual performance. Brain. 2002;**125**: 812-822

[40] Moser T, Dosch J-C, Moussaoui A, Dietemann J-L. Wrist ligament tears: Evaluation of MRI and combined MDCT and MR arthrography. American Journal of Roentgenology. 2007;**188**:1278-1286

[41] Bashir A, Gray M, Hartke J, Burstein D. Nondestructive imaging of human cartilage glycosaminoglycan concentration by MRI. Magnetic Resonance in Medicine. 1999;**41**:857-865

[42] Westbrook C, Roth CK, Talbot J. MRI in Practice. 4th ed. London: John Wiley & Sons, Inc.; 2011

[43] Brown RW, Haacke EM, Cheng Y-CN, Thompson MR, Venkatesan R. Resonance Imaging: Physical Principles and Sequence Design. 2nd ed. Wiley Blackwell; 2014

[44] Gore JC, Kennan RP. Physical and physiological basis of magnetic relaxation. In: Stark DD, Bradley WG, editors. Magnetic Resonance Imaging. 3rd ed. Vol. 1. New York: C.V. Mosby Publishing Co; 1999. pp. 33-42

[45] Jeong Y, Sook Hwang H, Na K. Theranostics and contrast agents for magnetic resonance imaging. Biomaterials Research. 2018;**22**:20

[46] Nelson KL, Gifford LM, Lauber-Huber C, Gross CA, Lasser TA. Clinical safety of gadopentetate dimeglumine. Radiology. 1995;**196**:439-443

[47] Gerald CF, Laurent S. Classification and basic properties of contrast agents for magnetic resonance imaging. Contrast Media & Molecular Imaging. 2009;**4**:1-23

[48] Herborn CU, Honold E, Wolf M, Kemper J, Kinner S, Adam G, et al. Clinical safety and diagnostic value of the gadolinium chelate gadoterate meglumine (Gd-DOTA). Investigative Radiology. 2007;**42**:58-62

[49] Strijkers GJ, Mulder WJ, Van Tilborg GA, Nicolay K. MRI contrast agents: Current status and future perspectives. Anti-Cancer Agents in Medicinal Chemistry. 2007;**7**(3):291-305

[50] Van Montfoort JE, Stieger B, Meijer DK, Weinmann H-J, Meier PJ, Fattinger KE. Hepatic uptake of the magnetic resonance imaging contrast agent gadoxetate by the organic anion transporting polypeptide Oatp1. The Journal of Pharmacology and Experimental Therapeutics. 1999;**290**: 153-157

[51] Tanaka H, Tanigawa T, Suzuki M, Otsuka K, Inafuku S. Effects of MRI contrast agents (Omniscan™) on vestibular end organs. Acta Oto-Laryngologica. 2010;**130**:17-24

[52] Kirchin MA, Pirovano GP, Spinazzi A. Gadobenate dimeglumine (Gd-BOPTA): An overview. Investigative Radiology. 1998;**33**: 798-809

[53] Runge VM, Kirsch JE, Burke VJ, Price AC, Nelson KL, Thomas GS, et al.

- High-dose gadoteridol in MR imaging of intracranial neoplasms. *Journal of Magnetic Resonance Imaging*. 1992;**2**: 9-18
- [54] Kim RJ, Albert TS, Wible JH, Elliott MD, Allen JC, Lee JC, et al. Performance of delayed-enhancement magnetic resonance imaging with gadoversetamide contrast for the detection and assessment of myocardial infarction: An international, multicenter, double-blinded, randomized trial. *Circulation*. 2008;**117**: 629-637
- [55] Staks T, Schuhmann-Giampieri G, Frenzel T, Weinmann H-J, Lange L, Platzek J. Pharmacokinetics, dose proportionality, and tolerability of gadobutrol after single intravenous injection in healthy volunteers. *Investigative Radiology*. 1994;**29**: 709-715
- [56] de Haën C, Anelli PL, Lorusso V, Morisetti A, Maggioni F, Zheng J, et al. Gadocoletic acid trisodium salt (b22956/1): A new blood pool magnetic resonance contrast agent with application in coronary angiography. *Investigative Radiology*. 2006;**41**: 279-291
- [57] Hompland T, Ellingsen C, Rofstad EK. Preclinical evaluation of Gd-DTPA and gadomelitol as contrast agents in DCE-MRI of cervical carcinoma interstitial fluid pressure. *BMC Cancer*. 2012;**12**:544
- [58] Bjørnerud A, Johansson LO, Ahlström H. Pre-clinical results with Clariscan™ (NC100150 injection); experience from different disease models. *Magma*. 2001;**12**:99-103
- [59] Lee N, Hyeon T. Designed synthesis of uniformly sized iron oxide nanoparticles for efficient magnetic resonance imaging contrast agents. *Chemical Society*. 2012;**41**:2575-2589
- [60] Clement O, Siauve N, Cuénod C-A, Frija G. Liver imaging with ferumoxides (Feridex): Fundamentals, controversies, and practical aspects. *Topics in Magnetic Resonance Imaging*. 1998;**9**: 167-182
- [61] Bonnemain B. Superparamagnetic agents in magnetic resonance imaging: Physicochemical characteristics and clinical applications a review. *Journal of Drug Targeting*. 1998;**6**:167-174
- [62] Sigal R, Vogl T, Casselman J, Moulin G, Veillon F, Hermans R, et al. Lymph node metastases from head and neck squamous cell carcinoma: MR imaging with ultrasmall superparamagnetic iron oxide particles (Sinerem MR)—results of a phase-III multicenter clinical trial. *European Radiology*. 2002;**12**:1104-1113
- [63] Reimer P, Balzer T. Ferucarbotran (Resovist): A new clinically approved RES specific contrast agent for contrast-enhanced MRI of the liver: Properties, clinical development, and applications. *European Radiology*. 2003;**13**:1266-1276
- [64] Lusic H, Grinstaff MW. X-ray-computed tomography contrast agents. *Chemical Reviews*. 2013;**113**(3): 1641-1666
- [65] Kalender WA. *Computed Tomography: Fundamentals, System Technology, Image Quality, Applications*. 3rd ed. Munich, Germany: Publicis; 2011
- [66] Lindsten J, editor. *Nobel Lectures: Physiology or Medicine 1971–1980*. Vol. 1. Singapore: World Scientific Publishing Co.; 1992
- [67] Yu S, Watson AD. Metal-based X-ray contrast media. *Chemical Reviews*. 1999;**99**:2353-2377
- [68] Janon EA. Gadolinium-DPTA: A radiographic contrast agent. *American Journal of Roentgenology*. 1989;**152**:1348

- [69] Engelbrecht V, Koch JA, Rassek M, Modder U. Magnetic resonance tomography and localized proton spectroscopy in 2 siblings with Canavan's disease. *RöFo: Fortschritte auf dem Gebiete der Röntgenstrahlen und der Nuklearmedizin*. 1996;**165**:24
- [70] Fobbe F, Wachter F, Wagner S. Arterial angiography in high-kilovoltage technique with gadolinium as the contrast agent: First clinical experience. *European Radiology*. 1996;**6**:224
- [71] Staks T, Schuhmann-Giampieri G, Frenzel T, Weinmann HJ, Lange L, Platzek J. Pharmacokinetics, dose proportionality, and tolerability of gadobutrol after single intravenous injection in healthy volunteers. *Investigative Radiology*. 1994;**29**:709
- [72] Bonvento MJ, Moore WH, Button TM, Weinmann HJ, Yakupov R, Dilmanian FACT. Angiography with gadolinium-based contrast media. *Academic Radiology*. 2006;**13**(8): 979-985
- [73] Schumann-Giampieri G, Mahler M, Roll G, Maibauer R, Schmitz S. Pharmacokinetics of the liver-specific contrast agent Gd-EOB-DTPA in relation to contrast-enhanced liver imaging in humans. *Journal of Clinical Pharmacology*. 1997;**37**:587
- [74] Huang D, Swanson EA, Lin CP, Schuman JS, Stinson WG, Chang W, et al. Optical coherence tomography. *Science*. 1991;**254**(5035):1178-1181
- [75] Fujimoto JG, Pitris C, Boppart SA, Brezinski ME. Optical coherence tomography: An emerging technology for biomedical imaging and optical biopsy. *Neoplasia*. 2000;**2**:9-25
- [76] Oldenburg A, Toublan F, Suslick K, Wei A, Boppart S. Magnetomotive contrast for in vivo optical coherence tomography. *Optics Express*. 2005; **13**(17):6597-6614
- [77] Oldenburg AL, Gunther JR, Boppart SA. Imaging magnetically labeled cells with magnetomotive optical coherence tomography. *Optics Letters*. 2005;**30**(7):747
- [78] Widder KJ, Senyei AE, Scarpelli DG. Magnetic microspheres: A model system for site-specific drug delivery in vivo. *Experimental Biology and Medicine*. 1978;**158**(2):141-146
- [79] Alexiou C, Jurgons R, Schmid R, Hilpert A, Bergemann C, Parak F, et al. In vitro and in vivo investigations of targeted chemotherapy with magnetic nanoparticles. *Journal of Magnetism and Magnetic Materials*. 2005;**293**(1): 389-393
- [80] Zhang X, Le T-A, Yoon J. Development of a real-time imaging-based guidance system of magnetic nanoparticles for targeted drug delivery. *Journal of Magnetism and Magnetic Materials*. 2017;**427**:345-351
- [81] Al-Jamal KT, Bai J, Wang JT-W, Protti A, Southern P, Bogart L, et al. Magnetic drug targeting: Preclinical in vivo studies, mathematical modeling, and extrapolation to humans. *Nano Letters*. 2016;**16**(9):5652
- [82] Cherry EM, Maxim PG, Eaton JK. Particle size, magnetic field, and blood velocity effects on particle retention in magnetic drug targeting. *Medical Physics*. 2010;**37**(1):175-182
- [83] Alexiou C, Arnold W, Klein R, Parak F, Hulin P, Bergemann C, et al. Locoregional cancer treatment with magnetic drug targeting. *Cancer Research*. 2000;**60**(23):6641-6648
- [84] Derfus AM, Von Maltzahn G, Harris TJ, Duza T, Vecchio KS, Ruoslahti E, et al. Remotely triggered release from magnetic nanoparticles. *Advanced Materials*. 2007;**19**(22): 3932-3936

- [85] Hu S-H, Liu T-Y, Liu D-M, Chen S-Y. Controlled pulsatile drug release from a ferrogel by a high-frequency magnetic field. *Macromolecules*. 2007;**40**: 6786-6788
- [86] Kim D-H, Nikles DE, Johnson DT, Brazel CS. Heat generation of aqueously dispersed CoFe₂O₄ nanoparticles as heating agents for magnetically activated drug delivery and hyperthermia. *Journal of Magnetism and Magnetic Materials*. 2008;**320**: 2390-2396
- [87] Braddock M. *Nanomedicines: Design, Delivery, and Detection*. Cambridge: RSC; 2016
- [88] Alexiou C, Schmidt A, Klein R, Hulin P, Bergemann C, Arnold W. Magnetic drug targeting: Biodistribution and dependency on magnetic field strength. *Journal of Magnetism and Magnetic Materials*. 2002;**252**(1-3): 363-366
- [89] Mahmoudi M, Simchi A, Imani M, Milani AS, Stroeve P. Optimal design and characterization of superparamagnetic iron oxide nanoparticles coated with polyvinyl alcohol for targeted delivery and imaging. *The Journal of Physical Chemistry. B*. 2008;**112**(46): 14470
- [90] Senyei A, Widder K, Czerlinski G. Magnetic guidance of drug-carrying microspheres. *Journal of Applied Physics*. 1978;**49**(6):3578-3583
- [91] Gregory TS, Wu KJ, Yu J, Box JB, Cheng R, Mao L, et al. Magneto-hydrodynamic-driven design of microscopic endocapsules in MRI. *IEEE/ASME Transactions on Mechatronics*. 2015;**20**(6):2691-2698
- [92] Eguchi H, Umemura M, Kurotani R, Fukumura H, Sato I, Kim J-H, et al. A magnetic anti-cancer compound for magnet-guided delivery and magnetic resonance imaging. *Scientific Reports*. 2015;**5**
- [93] Sato I, Umemura M, Mitsudo K, Fukumura H, Kim J-H, Hoshino Y, et al. Simultaneous hyperthermia-chemotherapy with controlled drug delivery using single-drug nanoparticles. *Scientific Reports*. 2016;**6**(1)
- [94] Ohtake M, Umemura M, Sato I, Akimoto T, Oda K, Nagasako A, et al. Hyperthermia and chemotherapy using Fe(Salen) nanoparticles might impact glioblastoma treatment. *Scientific Reports*. 2017;**7**
- [95] Chen P, Cui B, Bu Y, Yang Z, Wang Y. Synthesis and characterization of mesoporous and hollow-mesoporous M_xFe_{3-x}O₄ (M = Mg, Mn, Fe, Co, Ni, Cu, Zn) microspheres for microwave-triggered controllable drug delivery. *Journal of Nanoparticle Research*. 2017;**19**(12):1-11
- [96] Wang G, Zhao D, Li N, Wang X, Ma Y. Drug-loaded poly(ϵ -caprolactone)/Fe₃O₄ composite microspheres for magnetic resonance imaging and controlled drug delivery. *Journal of Magnetism and Magnetic Materials*. 2018;**456**:316-323
- [97] Zhang F, Zhao L, Wang S, Yang J, Lu G, Luo N, et al. Construction of a biomimetic magnetosome and its application as a siRNA carrier for high-performance anticancer therapy. *Advanced Functional Materials*. 2018;**28**(1)
- [98] Zheng S, Han J, Jin Z, Kim C-S, Park S, Kim K-P, et al. Dual tumor-targeted multifunctional magnetic hyaluronic acid micelles for enhanced MR imaging and combined photothermal-chemotherapy. *Colloids Surfaces B Biointerfaces*. 2018;**164**: 424-435
- [99] Park B-W, Zhuang J, Yasa O, Sitti M. Multifunctional bacteria-driven

- microswimmers for targeted active drug delivery. *ACS Nano*. 2017;**11**(9):8910
- [100] Xu H, Medina-Sánchez M, Magdanz V, Schwarz L, Hebenstreit F, Schmidt OG. Sperm-hybrid micromotor for targeted drug delivery. *ACS Nano*. 2018;**12**(1):327-337
- [101] Kralj S, Potrc T, Kocbek P, Marchesan S, Makovec D. Design and fabrication of magnetically responsive nanocarriers for drug delivery. *Current Medicinal Chemistry*. 2017;**24**(5):454-469
- [102] Häfeli UO, Pauer GJ. In vitro and in vivo toxicity of magnetic microspheres. *Journal of Magnetism and Magnetic Materials*. 1999;**194**(1):76-82
- [103] Moghimi SM, Hunter A, Murray J. Long-circulating and target-specific nanoparticles: Theory to practice. *Pharmacological Reviews*. 2001;**53**(2):283-318
- [104] Fernández-Pacheco R, Marquina C, Gabriel Valdivia J, Gutiérrez M, Soledad Romero M, Cornudella R, et al. Magnetic nanoparticles for local drug delivery using magnetic implants. *Journal of Magnetism and Magnetic Materials*. 2007;**311**(1):318-322
- [105] Polyak B, Fishbein I, Chorny M, Alferiev I, Williams D, Yellen B, et al. High field gradient targeting of magnetic nanoparticle-loaded endothelial cells to the surfaces of steel stents. *Proceedings of the National Academy of Sciences*. 2008;**105**(2):698
- [106] El-Sherbiny I, Elbaz N, Sedki M, Elgammal A, Yacoub M. Magnetic nanoparticles-based drug and gene delivery systems for the treatment of pulmonary diseases. *Nanomedicine*. 2017;**12**(4):387-402
- [107] Price DN, Stromberg LR, Kunda NK, Muttli P. In vivo pulmonary delivery and magnetic-targeting of dry powder nano-in-microparticles. *Molecular Pharmaceutics*. 2017;**14**(12):4741-4750
- [108] Li D, Ren Y. High-gradient magnetic field for magnetic nanoparticles drug delivery system. *IEEE Transactions on Applied Superconductivity*. 2018;**28**(6):1-7
- [109] Kohler N, Sun C, Wang J, Zhang M. Methotrexate-modified superparamagnetic nanoparticles and their intracellular uptake into human cancer cells. *Langmuir*. 2005;**21**(19):8858
- [110] Jain T, Morales MA, Sahoo S, Leslie-Pelecky D, Labhasetwar V. Iron oxide nanoparticles for sustained delivery of anticancer agents. *Molecular Pharmaceutics*. 2005;**2**(3):194-205
- [111] Wickline SA, Neubauer AM, Winter PM, Caruthers SD, Lanza GM. Molecular imaging and therapy of atherosclerosis with targeted nanoparticles, *Journal of Magnetic Resonance Imaging*. 2007;**25**:667-680
- [112] Jang J, Lee SS. Theoretical and experimental study of MHD (magneto hydrodynamic) micropump. *Sensors and Actuators A: Physical*. 2000;**80**(1):84-89
- [113] Choi SUS, Eastman JA. Enhancing thermal conductivity of fluids with nanoparticles. In: Energy. USDO, editor. *Int Mech Eng Congr Exhib San Fr*. 1995
- [114] Nisar A, Afzulpurkar N, Mahaisavariya B, Tuantranont A. MEMS-based micropumps in drug delivery and biomedical applications. *Sensors and Actuators B: Chemical*. 2008;**130**(2):917-942
- [115] Huang L, Wang W, Murphy MC, Lian K, Ling Z. LIGA fabrication and test of a DC type magneto hydrodynamic

(MHD) micropump. *Microsystem Technologies*. 2000;**6**(6):235-240

[116] Heng K-H, Wang W, Murphy MC, Lian K. UV-LIGA microfabrication and test of an ac-type micropump based on the magnetohydrodynamic (MHD) principle. In: *SPIE Proceedings*. Vol. 4177. 2000. pp. 161-171

[117] Lemoff AV, Lee AP. An AC magnetohydrodynamic micropump. *Sensors and Actuators B: Chemical*. 2000;**63**(3):178-185

[118] Wang Y-N, Fu L-M. Micropumps and biomedical applications—A review. *Microelectronic Engineering*. 2018;**195**: 121-138

[119] Abhari F, Jaafar H, Yunus NAM. A comprehensive study of micropumps technologies. *International Journal Of Electrochemical Science*. 2012;**7**: 9765-9780

[120] Gregory TS, Cheng R, Tang G, Mao L, Tse ZTH. The magnetohydrodynamic effect and its associated material designs for biomedical applications: A state-of-the-art review. *Advanced Functional Materials*. 2016;**26**(22):3942-3952

[121] Hola K, Markova Z, Zoppellaro G, Tucek J, Zboril R. Tailored functionalization of iron oxide nanoparticles for MRI, drug delivery, magnetic separation and immobilization of substances. *Biotechnology Advances*. 2015;**33**(6):1162-1176

[122] Zhou X, Gao M, Gui L. A liquid-metal based spiral magnetohydrodynamics micropump. *Micromachines*. 2017;**8**:365

[123] Bau HH, Zhu J, Qian S, Xiang YA. Magneto-hydrodynamic microfluidic network. In: *Proceedings ASME International Mechanical Engineering Congress & Exposition; New Orleans*. 2002. p. 33559

[124] Bau HH, Zhu J, Qian S, Xiang Y. A magneto-hydrodynamically controlled fluidic network. *Sensors and Actuators B*. 2003;**88**:207-218

[125] Qian S, Bau HH. Magneto-hydrodynamic based microfluidics. *Mechanics Research Communications*. 2009;**36**(1):10-21

[126] Gleeson JP, West J. Magnetohydrodynamic micromixing. *Technical Proceedings of the International Conference on Modeling and Simulation of Microsystems*. 2002: 318-321

[127] Gleeson JP, Roche OM, West J, Gelb A. Modeling annular micromixers. *SIAM Journal of Applied Mathematics*. 2004;**64**:1294-1310